Int. J. Environ. Sci. Technol. (2015) 12:3189–3212
DOI 10.1007/s13762-015-0752-y

ORIGINAL PAPER

Control of style-of-faulting on spatial pattern of earthquake-triggered landslides

T. Gorum · E. J. M. Carranza

Received: 9 June 2014 / Revised: 12 December 2014 / Accepted: 3 January 2015 / Published online: 20 January 2015

Abstract Predictive mapping of susceptibility to earthquake-triggered landslides (ETLs) commonly uses distance to fault as spatial predictor, regardless of style-of-faulting. Here, we examined the hypothesis that the spatial pattern of ETLs is influenced by style-of-faulting based on distance distribution analysis and Fry analysis. The Yingxiu–Beichuan fault (YBF) in China and a huge number of landslides that ruptured and occurred, respectively, during the 2008 Wenchuan earthquake permitted this study because the style-of-faulting along the YBF varied from its southern to northern parts (i.e. mainly thrust-slip in the southern part, oblique-slip in the central part and mainly strike-slip in the northern part). On the YBF hanging-wall, ETLs at 4.4–4.7 and 10.3–11.5 km from the YBF are likely associated with strike- and thrust-slips, respectively. On the southern and central parts of the hanging-wall, ETLs at 7.5–8 km from the YBF are likely associated with oblique-slips. These findings indicate that the spatial pattern of ETLs is influenced by style-of-faulting. Based on knowledge about the style-of-faulting and by using evidential belief functions to create a predictor map based on proximity to faults, we obtained higher landslide prediction accuracy than by using unclassified faults. When distance from unclassified parts of the YBF is used as predictor, the prediction accuracy is 80 %; when distance from parts of the YBF, classified according to style-of-faulting, is used as predictor, the prediction accuracy is 93 %. Therefore, mapping and classification of faults and proper spatial representation of fault control on occurrence of ETLs are important in predictive mapping of susceptibility to ETLs.

Keywords Distance distribution analysis · Fry analysis · Evidential belief functions · Geographic information system · Yingxiu–Beichuan fault · 2008 Wenchuan earthquake

T. Gorum
University of Twente, P.O. Box 217, 7500 AE Enschede, The Netherlands

T. Gorum
Yildiz Technical University, Esenler, 34220 Istanbul, Turkey

E. J. M. Carranza (✉)
James Cook University, Townsville, QLD 4811, Australia
e-mail: john.carranza@jcu.edu.au

Introduction

Landslides triggered by earthquakes are significant natural hazards to human life and property in many areas of the world. Predicting where earthquake-triggered landslides (ETLs) are likely to occur in relation to future earthquakes is difficult because scientifically reproducible predictions of where and when earthquakes will occur cannot be made yet. Nevertheless, as most earthquakes are associated with faults, many previous studies in predictive mapping of susceptibility to occurrence of ETLs (e.g. Bai et al. 2014; Jaafari et al. 2014; Pourghasemi et al. 2014; Regmi et al. 2014; Zhao et al. 2014) commonly use distance to (or from) every mapped fault as a spatial predictor, regardless of either orientation or style-of-faulting (i.e. strike-slip, dip-slip or oblique-slip). Implicit in this practice is the notion that every fault has equal influence on landslide occurrence. However, Ghosh and Carranza (2010) analysed the spatial pattern of landslides to determine which sets of faults, according to their strikes, are useful predictors of landslide susceptibility. They then showed that, compared with using distance to every fault (i.e. of various strikes), using distance to sets of faults of certain strikes and having positive spatial associations with

landslides yields a better predictive map of landslide susceptibility. Thus, as Dai et al. (2011) remind us, studying '…the spatial pattern of landslides triggered by an earthquake is important in understanding what areas may be susceptible to landsliding in future earthquakes'.

In the last three decades, various studies have contributed to the understanding of susceptibility to landsliding associated with earthquakes by studying spatial patterns of ETLs in relation to earthquake magnitude (e.g. Keefer 1984, 1993, 1994, 2002; Chen et al. 2012; Das et al. 2013; Xu and Xu 2014), ground motion parameters (e.g. Keefer 1984; Jibson and Keefer 1993; Eberhart-Phillips et al. 2003; Wu and Lin 2009; Kaiser et al. 2012; Huang and Fan 2013; Gorum et al. 2014), distance from epicentre or from fault rupture (e.g. Keefer 1984; Crozier et al. 1995; Eberhart-Phillips et al. 2003; Song et al. 2012; Li et al. 2013a, b; Yin 2014), geological properties such as lithology and soil (e.g. Keefer 1984; Holzer 1994; Shou and Wang 2003; Malamud et al. 2004; Huang et al. 2014), geomorphic features such rivers and ridges (Hewitt 1983; Yang 1992; Chang and Slaymaker 2002; Xu et al. 2012; Xu and Xu 2013; Pourghasemi et al. 2014) and topographic variables such as slope gradient and curvature (Hewitt 1983; Jibson and Keefer 1993; Chang and Slaymaker 2002; Xu et al. 2012; Xu and Xu 2013, 2014). Among these studies, those in the first two of the last three decades (e.g. Hewitt 1983; Keefer 1984, 1993, 1994, 2002; Jibson and Keefer 1993; Eberhart-Phillips et al. 2003; Shou and Wang 2003) have formed the bases of various studies in using a geographic information system (GIS) for predictive mapping of susceptibility to occurrence of ETLs (e.g. Bai et al. 2014; Jaafari et al. 2014; Pourghasemi et al. 2014; Regmi et al. 2014; Zhao et al. 2014).

The studies cited in the preceding paragraph only provide implicit relationships between spatial patterns of ETLs and style-of-faulting (i.e. based on slip direction). However, differences in style-of-faulting represent variations in distribution of stress and vice versa, which influence variations in seismicity or ground motion parameters (Wei et al. 2012; Tesón et al. 2013; Bradley et al. 2014). Accordingly, different styles-of-faulting have different influence on geomorphic processes such as landsliding (e.g. Wu and Chen 2011; Huang et al. 2012; Huang and Fan 2013; Xu and Xu 2014). Based on two- and three-dimensional dynamic simulations of dipping faults, for the same initial stress magnitude, thrust (or reverse dip-slip) faults can produce much higher fault and ground motion than normal and strike-slip faults (Oglesby and Day 2002; Beavan et al. 2012; Shi and Day 2013; Gabuchian et al. 2014). Considering that landslides are important components of a geomorphic system, Scheidegger (2001) emphasized that ongoing tectonic movements, especially neo-tectonic processes, have much more profound influence on geomorphic systems and, thus, on landslide formation than the generally assumed factors of geomorphic development. Later studies elsewhere, based on two- and three-dimensional dynamic simulations of dipping faults, show that, for the same initial stress magnitude, thrust (or reverse dip-slip) faults can produce much higher fault and ground motion than normal and strike-slip faults (Nielsen 1998; Shi et al. 1998; Oglesby et al. 1998, 2000a, b; Oglesby and Day 2002). However, while the relationship of ETLs with various factors is relatively well known, little is known about the role of fault slips and orientations in co-seismic landsliding and their influence on the spatial pattern of ETLs. Therefore, analysis of the spatial pattern of ETLs in relation to style-of-faulting would contribute further to the understanding of susceptibility to occurrence of ETLs.

In this paper, we examine the hypothesis that the spatial pattern of ETLs is influenced by style-of-faulting. To do so, we chose the 240-km-long Yingxiu–Beichuan fault (YBF) as reference because of two reasons. Firstly, it was associated with the 2008 Wenchuan earthquake that triggered a huge number of landslides (Ouimet 2009; Chigira et al. 2010; Dai et al. 2011; Tang et al. 2010; Yin et al. 2010; Zhuang et al. 2010; Xu and Xu 2013; Xu et al. 2012, 2014) (Fig. 1). Secondly, the style-of-faulting along the YBF, from its southern to northern parts, varied from mainly thrust-slip to mainly strike-slip (Wang et al. 2009, 2010; Lin et al. 2009; Wan and Shen 2010) (Fig. 2). Based on these two reasons, we examined the above hypothesis by investigating two research questions. Firstly, given that style-of-faulting can vary along a fault, can we classify that fault according to predominant style-of-faulting based on the spatial pattern of associated ETLs? This question bears the importance of mapping and classification of faults prior to predictive mapping of susceptibility to occurrence of ETLs. Secondly, granted that parts of a fault can be classified according to predominant style-of-faulting, how does the spatial pattern of associated ETLs vary with respect to predominant style-of-faulting? This question bears the importance of proper representation of predictors in predictive mapping of susceptibility to occurrence of ETLs. Thus, we also show here that using classified faults, rather than using un-classified faults, provides for better spatial representation of fault control as a predictor of susceptibility to occurrence of ETLs. This study, using the ETL inventory of Gorum et al. (2011), was conducted from 2011 to 2012 in the University of Twente (Netherlands).

Study area

Tectonic setting and the 2008 earthquake

The 12 May 2008 M_w 7.9 Wenchuan earthquake occurred in the NE-trending Longmenshan thrust fault belt along the

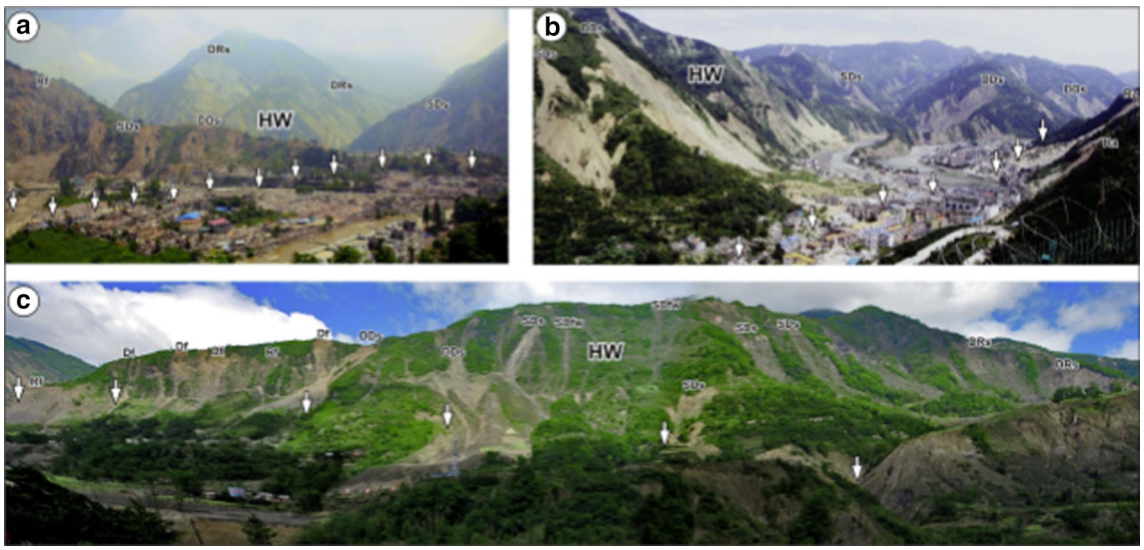

Fig. 1 Photographs (see Fig. 2 for locations) of earthquake-induced landslides on the hanging wall (HW) with different slip components of the Yingxiu–Beichuan fault surface rupture (locations indicated by *white vertical arrows*). Earthquake-induced landslides on hanging-wall with **a** predominantly thrust-slip components at Yingxiu, **b** predominantly oblique-slip components at Beichuan and **c** predominantly strike-slip components at roughly 12 km N of Chenjiaba. *Ra* rock avalanche, *Rf* rockfall, *Ds* debris fall, *DRs* deep-seated rock slide, *DDs* deep-seated debris slide, *SDs* shallow debris slide, *SDfw* shallow debris flow

eastern margin of the Tibetan Plateau that borders with the Sichuan Basin (Fig. 2). This fault belt, a spectacular mountain range, has developed due to the convergence of the Tibetan Plateau with the Sichuan Basin since Late Triassic (Burchfiel et al. 1995; Li et al. 2003; Richardson et al. 2008). Because of that convergence, a complex package of rocks, including Triassic marine sedimentary rocks of the Songpan-Ganzi remnant ocean basin (Zhou and Graham 1996), was thrusted to the southeast over the margin of the South China block, creating a Late Triassic foreland basin. The fault belt consists of a series of active parallel thrusts (Fig. 2), among which the Wenchuan–Maowen fault, Yingxiu–Beichuan fault (YBF) and Pengguan fault (PF) are seismogenic (Li et al. 2003; Densmore et al. 2007).

The 2008 Wenchuan earthquake, which initiated close to the south end of the YBF and propagated unilaterally towards the NE for about 320 km (Wang et al. 2009; Xu et al. 2009), ruptured both the YBF (240 km long) and PF (70 km long) (Fig. 2). Shen et al. (2009) showed that the rupture along the southern parts of the YBF has different geometry than the rupture along its northern parts from SW of Beichuan towards NE (Fig. 3). The north-west dips of the YBF are, on average, 43°–44° along its southern parts and increase to 49°–50° along its central parts approximately around Beichuan, and they are at least 55° to nearly vertical in its northern parts. These variations in the geometry of the YBF have corresponding variations in co-seismic slip directions and slip rates (Liu-Zeng et al. 2009; Xu et al. 2009).

Nakamura et al. (2010) and Zhao et al. (2010) showed that the rupture along the YBF was due to two major seismic sub-events (Fig. 2), one that occurred near Yingxiu had mainly thrust-slip components and the other that occurred near Beichuan had mainly right-lateral strike-slip components. Zhao et al. (2010) further showed that the Wenchuan earthquake consisted of five sub-events of $M_w \geq 7.3$ that occurred successively in time and space (Fig. 2). They also pointed out that the surface rupture consisted of two areas with large slips. One area with large slips was Dujiangyan–Mianzhu located 20–80 km NE from the epicentre. In this area, the rupture had large thrust-slips within depths of <15 km (Fig. 4). Around Mianzhu near Leigu, the thrust-slips converted to dextral strike-slips, which extended northwards along the YBF to Qingchuan forming another area, 140–260 km NE from the epicentre, with large slips within depths of <10 km (Fig. 4).

Several studies (e.g. Parsons et al. 2008; Lin et al. 2009; Liu-Zeng et al. 2009; Wang et al. 2010; Zhang et al. 2010; Fu et al. 2011; Li et al. 2013a, b; Wang et al. 2014) have shown that in the southern parts of the YBF thrust-slip components were larger than strike-slip components, whereas in the northern parts of the YBF strike-slip components were larger than thrust-slip components (Fig. 4). Northwards from Leigu, about 5 km SW of Beichuan, the dextral strike-slip components became roughly equal to, or

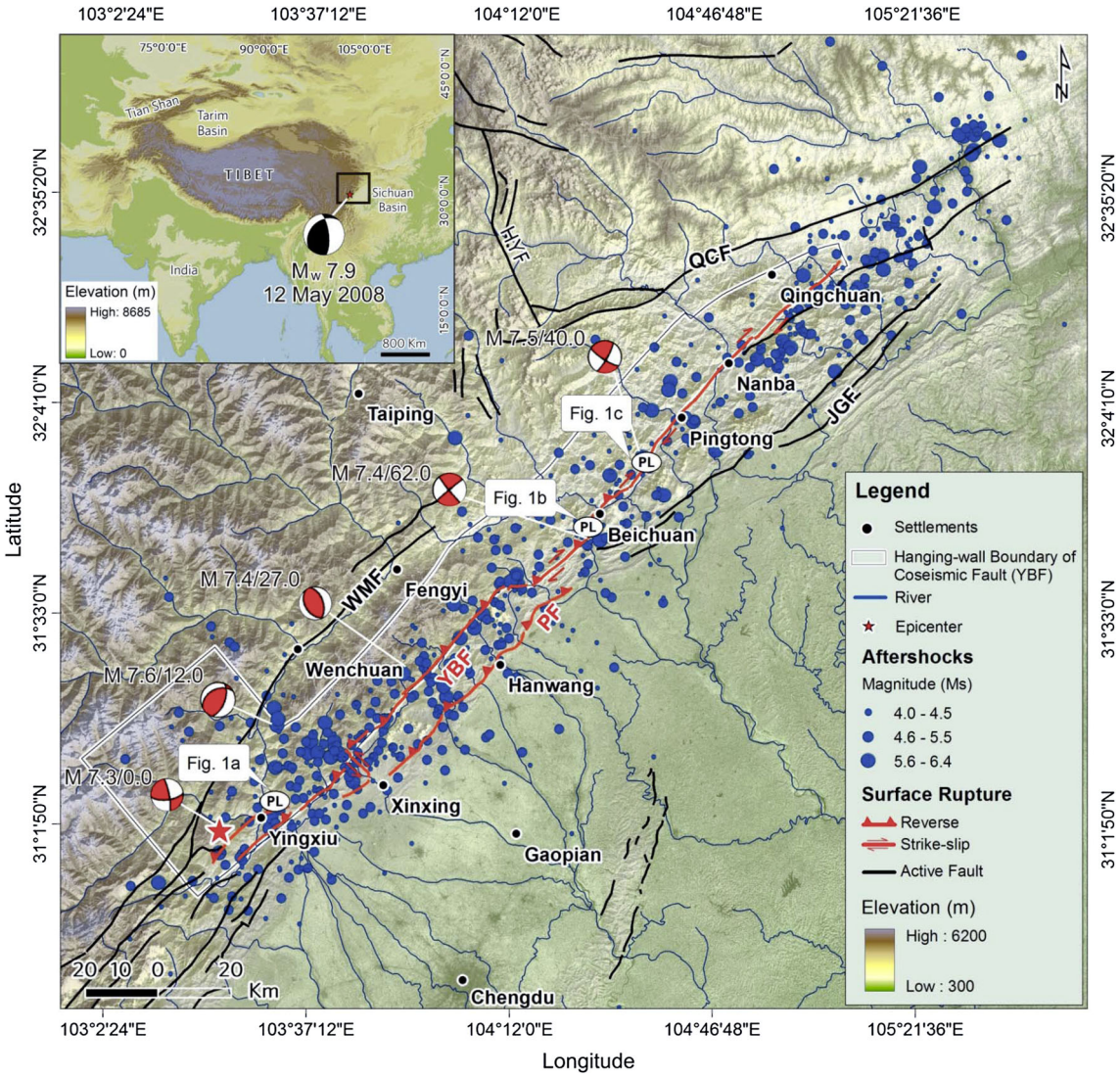

Fig. 2 Map of the Wenchuan earthquake fault surface rupture (from Xu et al. (2009)) and focal mechanisms (*black–white* 'beach ball') of the main 12 May 2008 earthquake (from USGS (2008)). The *map* shows also the moment tensor solutions of the earthquake and the distribution of sub-events (*red-white* 'beach ball'), their mechanisms and their time relative to the initial origin times (from Zhao et al. (2010). Traces of following faults are adopted from Xu et al. (2009): *WMF* Wenchuan–Maowen fault, *YBF* Yingxiu–Beichuan fault, *PF* Pengguan fault, *JGF* Jiangyou–Guanxian fault, *QCF* Qingchuan fault. *PL* location of photographs shown in Fig. 1

slightly larger than, the vertical offsets measured at many localities by Liu-Zeng et al. (2009) and Xu et al. (2009). The strike-slip components then increased fairly near Chenjiaba (10 km NE of Beichuan). The average vertical offset along the YBF was 3–4 m, with maxima of 6.5 ± 0.5 m at north of Beichuan (31°50′18.6″N, 104°28′3.6″E) in the northern parts and 6.2 ± 0.5 m at Yingxiu near the branching point in the southern parts (Xu et al. 2009). The maximum dextral strike-slip offset identified by Xu et al. (2009) was 4.9 ± 0.5 m at Pingtong (31°5′23.8″N, 103°36′56.9″E).

Earthquake-triggered landslides associated with the 2008 earthquake

The 2008 Wenchuan earthquake triggered and resulted in several tens of thousands of individual landslides of different types and sizes, which made it one of the most extreme catastrophes in terms of ETLs in the last century (Ouimet 2009; Chigira et al. 2010; Dai et al. 2011; Tang et al. 2010; Wang et al. 2010; Yin et al. 2010; Zhuang et al. 2010; Xu et al. 2014). The most common types of landslides associated with that seismic event were

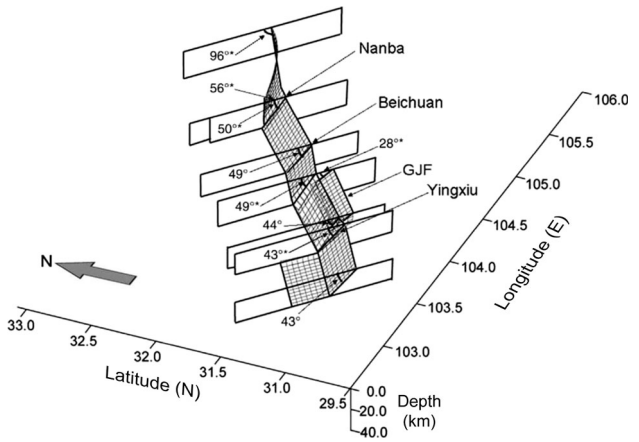

Fig. 3 Model geometry of the Yingxiu–Beichuan fault as viewed from SW at 45° elevation angle (adopted from Shen et al. 2009). Fault dip angle was assumed constant along dip and varies linearly along strike, with six dip angles at fault nodal points inverted in the solution by Shen et al. (2009)

rockfalls, rock avalanches and rock–debris slides (Chigira et al. 2010; Dai et al. 2011). Large and deep-seated landslides were quite common, especially close to the fault ruptures (Fig. 1), and they occurred mostly in the southern and central parts of the hanging-wall of the YBF, whereas smaller and shallow landslides occurred mainly on the hanging-wall of the YBF (Figs. 1, 5). Most of the landslides occurred, however, in highly fractured and jointed Precambrian crystalline and metamorphic rocks, in weakly cemented and weathered Cambrian sedimentary rocks and in pre-existing landslide deposits (Dai et al. 2011).

By processing and interpreting various pre- and post-earthquake, high spatial resolution satellite images (ASTER, 15 m; ALOS, 2.5 m; Cartosat-1, 2.5 m; SPOT-5, 2.5–5 m; IKONOS, 1–4 m), Gorum et al. (2011) identified 60,104 individual initiation points (or locations) of the landslides triggered by the 2008 Wenchuan earthquake (Fig. 5). This inventory of earthquake-triggered landslide initiation points was used by Gorum et al. (2011) to analyse the influence of the dynamic rupture processes on the distribution of ETLs associated with the 2008 Wenchuan earthquake. Based on this inventory of earthquake-triggered landslide initiation points, we can see that the ETLs were widely and densely distributed around the southern to

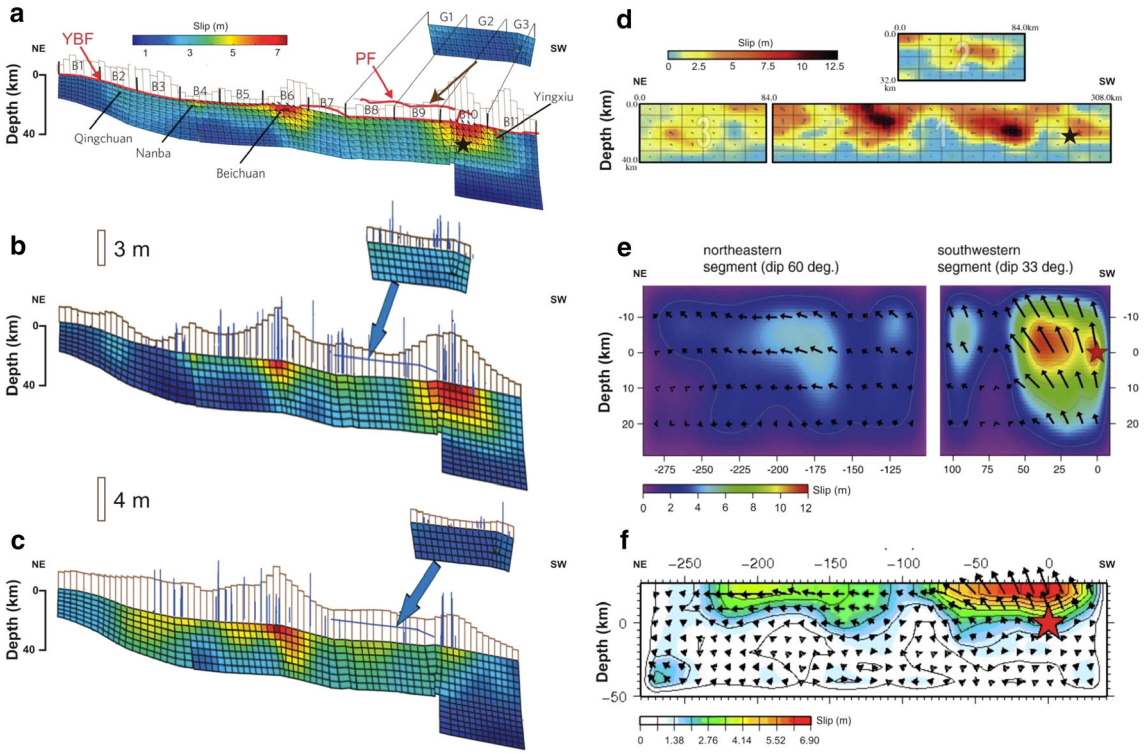

Fig. 4 Co-seismic slip distributions during the 2008 Wenchuan earthquake along the Yingxiu–Beichuan fault (YBF) according to **a**–**c** Shen et al. (2009), **d** Wang et al. (2008a, b), **e** Nakamura et al. (2010) and **f** Nishimura and Yagi (2008). Reverse-slip (**b**) and dextral-slip amplitudes (**c**) and model surface offsets (*columns*) are compared with field observations (*thin lines*; adopted from Xu et al. 2009). *PF* Pengguan fault

central parts of the YBF but narrowly and sparsely distributed around the northern parts of the YBF (Fig. 5a). In addition, the inventory of earthquake-triggered landslide initiation points indicates that about 70 % of the ETLs occurred in the area between Yingxiu and Beichuan (Fig. 5d, e), and this observation coheres with the high vertical slip rates measured by Liu-Zeng et al. (2009) and Xu et al. (2009) in that area (Fig. 5b). Moreover, the inventory of earthquake-triggered landslide initiation points of Gorum et al. (2011) indicates that about 60 % of the ETLs occurred on the hanging-wall of the YBF, whereas about 15 % of the ETLs occurred on the hanging-wall of the PF (Fig. 5a). The remaining 25 % of the ETLs occurred on slopes of deeply incised valleys much farther (about 25 km) to the west of the YBF or on the footwall of either the YBF or the PF (Fig. 5a).

Apparently, the distribution of the ETLs on the hanging-wall of the YBF was widest (up to about 17 km) in its southern part, intermediate (up to about 10 km) in its central part and narrowest (up to about 3.5 km) in its northern part (Fig. 5a). In the longitudinal swath profile (18 km wide and 240 km long) that we constructed on the hanging-wall of the YBF (Fig. 5d), the density of ETLs (number of landslide per km^2) decreases from south to north along strike of the surface rupture of this fault (Fig. 5d). On the hanging-wall of the YBF with predominantly thrust-slip component (PdTC), or in the area between Yingxiu and Beichuan where the vertical co-seismic offsets are relatively larger than the horizontal co-seismic offsets (Fig. 5b, c), the average density of ETLs is generally more than 20 km^{-2} with a maximum density of 54 km^{-2} (Fig. 5d). In contrast, on the hanging-wall of the

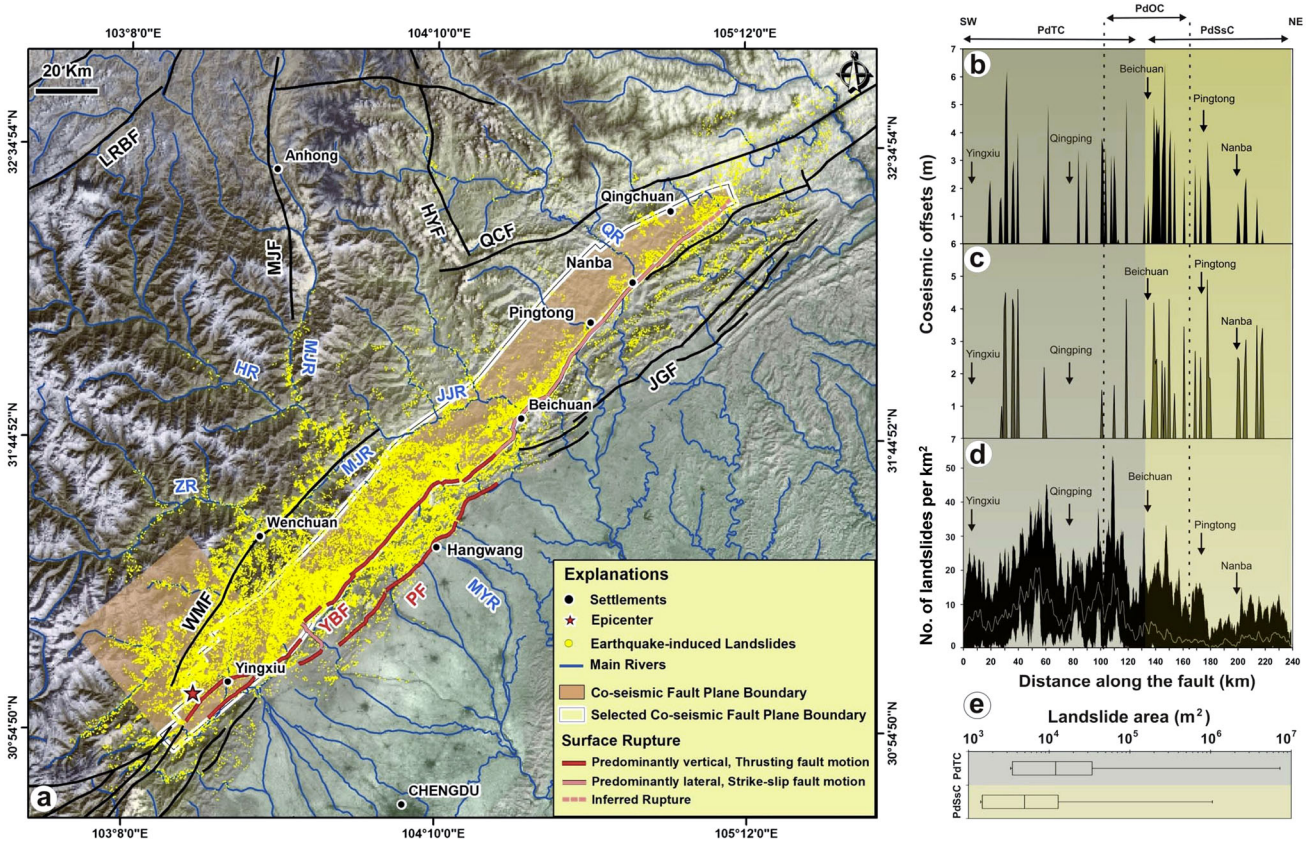

Fig. 5 Distribution of earthquake-induced landslides and co-seismic offsets along the Yingxiu–Beichuan fault (YBF) The *map* (**a**) contains 60,104 landslide initiation points (from Gorum et al. 2011). The vertical (**b**) and horizontal (**c**) co-seismic offsets, measured by Xu et al. (2009), show that the YBF can be divided into three parts depending on whether they have predominantly thrust components (PdTC), predominantly strike-slip components (PdSC) or predominantly oblique components (PdOC). The graph in (**d**) illustrates that, in the selected co-seismic fault plane boundary shown in (**a**), along-strike swath profile of earthquake-induced landslide density varies depending on the predominant fault slip components along the YBF. The *box-whisker plot* in (**e**) illustrates that, in the selected co-seismic fault plane boundary shown in (**a**), the total area affected by earthquake-induced landslides also varies depending on the predominant fault slip components along the YBF. In the *map*, the following rivers are indicated: *MJR* Minjiang River, *ZR* Zagunao River, *HR* Heishuehe River, *MYR* Mianyuan River, *JJR* Jianjiang River, *QR* Qingzhu River. For fault names in the *map*, see Fig. 1

YBF with predominantly strike-slip component (PdSsC), or in the area between Beichuan and Qingchuan where the horizontal co-seismic offsets are relatively larger than the vertical co-seismic offsets (Fig. 5b, c), the average density of ETLs is generally less than 15 km^{-2} with a maximum density of 30 km^{-2} (Fig. 5d). Moreover, ETLs on the hanging-wall of the YBF with PdTC have higher areal coverage than ETLs on the hanging-wall of the YBF with PdSsC (Fig. 3e). Finally, in the area between 30 km south and 30 km north of Beichuan, where horizontal co-seismic offsets and vertical co-seismic offsets are roughly equal (Figs. 4a–c, 5b, c), the YBF has a predominantly oblique-slip component (PdOC). On the hanging-wall of the YBF with PdOC, the average density of ETLs is lower than on the hanging-wall of the YBF with PdTC but is higher than on the hanging-wall of the YBF with PdSsC (Fig. 5d). The foregoing observations and initial analyses indicate, therefore, that the spatial pattern of ETLs depends on style-of-faulting. In the following section, we investigate dependency of spatial pattern of ETLs on style-of-faulting.

Materials and methods

To examine the hypothesis that the spatial pattern of ETLs is influenced by style-of-faulting, we investigated two research questions. Firstly, given that style-of-faulting can vary along a fault, can we classify that fault according to predominant style-of-faulting based on the spatial pattern of associated ETLs? Secondly, granted that parts of a fault can be classified according to predominant style-of-faulting, how does the spatial pattern of associated ETLs vary with respect to predominant style-of-faulting? To investigate these two research questions, we applied the distance distribution analysis (see "Distance distribution analysis of landslide distribution" section) to characterize the spatial pattern of ETLs and we investigated further our interpretations of the distance distribution analyses by application of Fry analysis (see "Fry analysis of landslide distribution" section). Finally, we applied evidential belief functions (see "Representation of fault control on susceptibility to landsliding" section) to test whether using classified faults, compared with using un-classified faults, improves prediction accuracy of landslide susceptibility mapping.

Distance distribution analysis of landslide distribution

In previous studies in the study area (Huang and Li 2009; Dai et al. 2011; Yin et al. 2010; Zhuang et al. 2010), the spatial pattern of ETLs with respect to distance from the YBF was characterized by the number or percentage of landslides (depicted as points) per unit of cumulative increasing area of its footwall or hanging-wall. This method is, however, inadequate for examining spatial dependency of a set of point objects on another set of objects. That is because spatial dependency is not associated with random chance and must be examined properly via probabilistic methods. Here, we applied the distance distribution analysis, which is a probabilistic method formalized by Berman (1977, 1986) for measuring spatial association between a set of point objects and another set of objects. The formalism of the distance distribution method is complex, and for details, the readers are referred directly to the seminal papers of Berman (1977, 1986); however, the following discussion for its application here is simplified.

The distance distribution analysis involves constructing two graphs. One graph [denoted as $D(L)$] represents cumulative relative frequency distribution of distances from a set of objects (e.g. surface ruptures along the YBF) to every location. The other graph [denoted as $D(NL)$] represents cumulative relative frequency distribution of distances from the same set of object(s) to locations of individual ETLs (depicted as points). In this study, the $D(L)$ is considered a non-random probability distribution of ETLs with respect to surface ruptures along the YBF, whereas the $D(NL)$ is considered a random probability distribution of (mostly) non-landslide locations with respect to the same set of spatial objects.

To determine whether ETLs are associated spatially with surface ruptures along the YBF, the $D(L)$ is compared with the $D(NL)$ by calculating the Kolmogorov–Smirnov statistic $D = D(L) - D(NL)$ (Berman 1977, 1986). The statistical significance of D can be evaluated through a Chi-square (χ^2) test (for details, see Chernoff and Lehmann 1954 or Plackett 1983). Positive and negative values of D represent how much the likelihood of earthquake-triggered landslide occurrence associated with surface ruptures along the YBF is, respectively, higher or lower than would be expected due to random chance. A value of $D \cong 0$ implies that ETLs under study lack spatial association with surface ruptures along the YBF. A value of $D > 0$ implies that ETLs under study have positive spatial association with surface ruptures along the YBF. A value of $D < 0$ implies that ETLs under study have negative spatial association with surface ruptures along the YBF. A positive, rather than negative, spatial association between a set of point objects and another set of objects is regarded as spatial dependence (Berman 1977, 1986). Thus, the highest peak in a graph of D versus distance (or the difference

curve) represents distance from reference objects within which there is optimum positive spatial association between those objects and a set of point objects.

Fry analysis of landslide distribution

Fry analysis (Fry 1979) is a graphical method of spatial autocorrelation analysis of a set of point objects (e.g. ETLs depicted on district- to regional-scale maps). The formalism of this method is complex, and for details, the readers are referred directly to the seminal papers of Fry (1979) and Hanna and Fry (1979); however, the following discussion for its application here is informal and simplified. The method translates point objects into a Fry plot by using every point as an origin for translation. On a map of point objects, N–S and E–W reference lines are drawn. On a second but empty map, N–S- and E–W-trending reference lines are also drawn and an origin for translation is marked at the intersection of an N–S reference line and an E–W reference line. The origin in the second map is placed on top of one of the points in the first map, the reference lines in both maps are kept parallel, and the positions of all the points are recorded in the second map. The origin in the second map is then placed on top of a different point in the first map, the reference lines in both maps are kept parallel, and the positions of all the points are recorded again in the second map. The procedure is repeated until all the points in the first map have been used as the origin in the second map. If the number of points is n, the number of point translations is n^2–n. These point translations, called Fry points, were developed originally to investigate strain and strain partitioning in rocks (Fry 1979; Hanna and Fry 1979).

Based on a Fry plot, a rose diagram can be created for visual analysis of trends between (a) all pairs of Fry points and (b) pairs of Fry points within specified distances from each other. The former analysis reveals trends that can be associated with regional-scale geological processes or are artefacts of the shape of study area, whereas the latter analysis reveals trends that can be associated with local-scale geological processes. Analysis of Fry points within specified distances from each other is, in this study, apt for studying trends in the spatial pattern of ETLs that are likely associated with style-of-faulting along earthquake faults. For this purpose, we considered to use minimum distance from every earthquake-triggered landslide within which there is probability of only one neighbour earthquake-triggered landslide. This minimum distance (60 m for the ETLs in the 21-km-wide zone on the hanging-wall of the YBF) can be determined via point pattern analysis (see Boots and Getis (1988) for details). We made that consideration because it is likely that any two ETLs, within that distance from each other, are controlled by the same process(es).

Representation of fault control on susceptibility to landsliding

Predictive mapping of susceptibility to landsliding requires representation and integration of known spatial factors as layers of evidence of that phenomenon. This means that a layer of evidence of landslide susceptibility should adequately capture the process involved and spatial association between landslides and a spatial factor (style-of-faulting). In this paper, we use data-driven evidential belief functions (EBFs), which are based on the Dempster–Shafer theory of belief (Dempster 1967; Shafer 1976) for representing degrees of belief that evidence supports a proposition and thus represents spatial association between evidence and phenomenon under study. The EBFs to be estimated are belief (*Bel*), disbelief (*Dis*) and uncertainty (*Unc*). *Bel* is a lower degree of belief in evidence with respect to a proposition. *Dis* is a degree of disbelief in evidence with respect to that proposition. *Unc* is 'ignorance' or 'doubt' in evidence with respect to that proposition. The sum $Bel + Unc + Dis$ for evidence with respect to any proposition is equal to 1 (i.e. maximum probability). *Unc* influences the relation between *Bel* and *Dis*. If $Unc = 0$ (i.e. complete knowledge about an evidence), $Bel + Dis = 1$ and the relation between *Bel* and *Dis* is binary (i.e. $Bel = 1 - Dis$ or $Dis = 1 - Bel$), as in the theory of probability. If $Unc = 1$ (i.e. complete ignorance about an evidence), *Bel* and *Dis* are both equal to zero, because, if there is complete uncertainty, there can be neither belief nor disbelief. Usually, however, *Unc* is neither equal to zero nor equal to one. If $0 < Unc < 1$, then $Bel = 1 - Dis - Unc$ or $Dis = 1 - Bel - Unc$, meaning that the relation between *Bel* and *Dis* is not binary because some uncertainty is present. Thus, one should estimate not only *Bel* but also *Dis* and *Unc* for any evidence (e.g. distance to fault) used to evaluate a proposition (e.g. 'this location is prone to earthquake-triggered landsliding').

Estimation of EBFs of evidence with respect to certain propositions has traditionally been knowledge driven (i.e. based on expert opinion), which is subjective because (a) no two experts will have the same opinion about an evidence for a certain proposition and (b) differentiating between and, thus, estimating *Dis* and *Unc* is conceptually difficult. However, Carranza and Hale (2003) have developed a method using a GIS for data-driven estimation of

EBFs of spatial evidence of mineral prospectivity. Details of data-driven estimation of EBFs are not given here, but can be found in Carranza and Castro (2006) or Ghosh and Carranza (2010), who used that method for predictive mapping of susceptibility to, respectively, distal lahar-inundation in Mount Pinatubo (Philippines) and rock sliding in Darjeeling Himalaya (India).

Results and discussion

Distance distribution analysis of landslide distribution

To examine the above-stated hypothesis without loss of generality, we applied the distance distribution analysis to characterize the spatial pattern of ETLs in a 240-km-long zone on the hanging-wall of the YBF (Fig. 5). This zone is the surface projection of the co-seismic fault plane boundary of the YBF (Figs. 4a, 5) defined by Shen et al. (2009), except that we disregard the south-western-most portion of this fault plane boundary because its surface projection coincides with the hanging-wall of the Wenchuan–Maowen fault (WMF). The jagged south-western boundary of the considered zone is due to the cell configurations used by Shen et al. (2009) (Fig. 4a–c). The western boundary of the considered zone is at most 21 km from the surface ruptures of the YBF. This distance is roughly the average of various reported widths of zones on the hanging-wall of the YBF with the highest density of ETLs (i.e. ~25–30 km (Ouimet 2009; Dai et al. 2011), 11.5 km (Yin et al. 2010), 15 km (Zhuang et al. 2010), 30 km (Chigira et al. 2010)). Thus, based on findings of previous studies in the area, we believe that constraining the examination of the above-stated hypothesis within the defined 240-km-long and 21-km-wide zone on the hanging-wall of the YBF is likely to give significant and interesting findings. In applying distance distribution analysis, we used a map unit cell size of 100 m to represent every location in the study area; thus, in the hanging-wall of the YBF, there are at least 400,000 unit cells, of which at least 28,000 unit cells contain at least one ETL. Because of these large numbers of unit cells, all the results of distance distribution analysis indicated statistically significant spatial patterns.

To investigate the first research question, we performed two sets of distance distribution analysis using distances not from the surface ruptures of the YBF but from (1) the north end of the hanging-wall of the YBF and (2) the south end of the hanging-wall of the YBF. The purpose of these analyses is to classify the parts of the hanging-wall of the YBF, in terms of style-of-faulting, with respect to variations in the spatial pattern of the ETLs from the north and south ends of the hanging-wall of the YBF. The analyses indicate relative paucity and relative abundance of ETLs, respectively, within and beyond 110 km of the north end of the hanging-wall of the YBF (Fig. 6a1). The analyses also indicate relative abundance and relative paucity of ETLs, respectively, within and beyond 130 km of the south end of the hanging-wall of the YBF (Fig. 6a2). These suggest that, about 18 km SSW to about 26 km W of Beichuan, slips along the hanging-wall of the YBF changed from mainly thrust-slip in the south to mainly strike-slip in the north (Fig. 6a3). We believe, nonetheless, that there was a zone between the southern and northern parts of the hanging-wall of the YBF wherein oblique-slips had roughly equal thrust- and strike-slip components. To examine this belief, we used the transition line in Fig. 6a3 as reference for another two sets of distance distribution analysis. The analysis shown in Fig. 6b1 indicates relative abundance of ETLs within 30 km from the transition line towards the north end of the hanging-wall of the YBF. The analysis shown in Fig. 6b2 indicates relative paucity of ETLs within 30 km from the transition line towards the south end of the hanging-wall of the YBF. The analyses shown in Fig. 6b1, b2 are consistent with the knowledge that the predominant styles of co-seismic movements in the southern, central and northern parts of the YBF were different (Fig. 6b3). The boundaries of these parts of the hanging-wall of the YBF as depicted in Fig. 6b3 are symbolic and not meant to portray where abrupt changes in style-of-faulting took place. However, the analyses suggest that the hanging-wall of the YBF can be divided into at least three sub-zones according to predominant style-of-faulting (Fig. 6b3), which are consistent with the analyses of Zhao et al. (2010) that the surface rupture along the YBF consisted of two large slip areas, one located 20–80 km NE from the epicentre (corresponding to our mainly thrust-slip southern part) and the other located 140–260 km NE from the epicentre (corresponding to our mainly strike-slip northern part). The analyses are also roughly consistent with fault slip distribution models (Nishimura and Yagi 2008; Wang et al. 2008a, b; Hao et al. 2009; Wang et al. 2010) (Fig. 4) and field-based offset measurements (Lin et al. 2009; Liu-Zeng et al. 2009; Xu et al. 2009) (Fig. 5c, d).

To investigate the second research question, we performed three sets of distance distribution analysis using distances from the surface ruptures of the YBF to every location and to landslide locations on the southern, central and northern parts of the hanging-wall of the YBF. The purpose of these analyses is to characterize the spatial

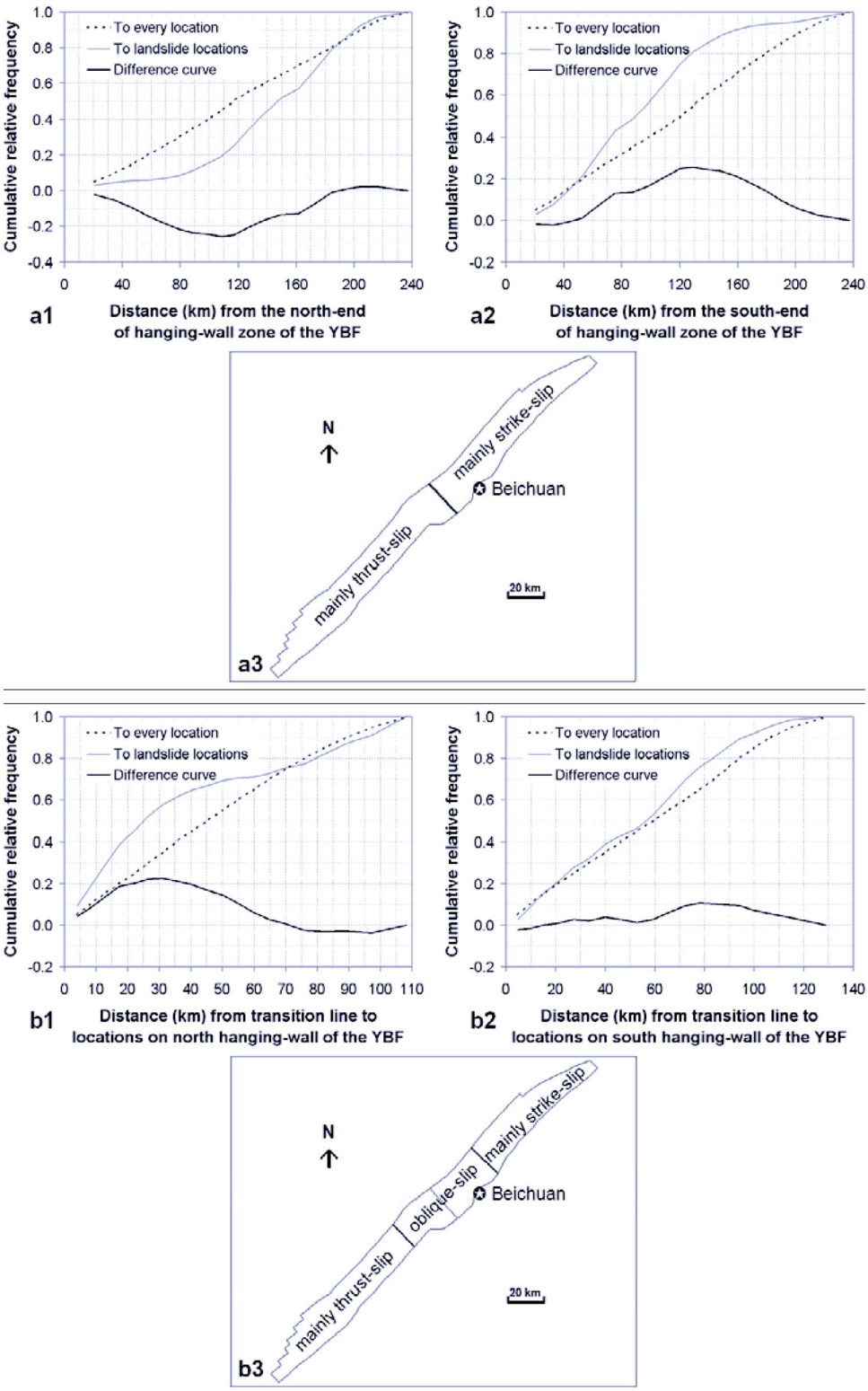

Fig. 6 Graphs of cumulative relative frequency of distances: to every location and to landslide locations from the **a1** north end of hanging-wall of the YBF and **a2** south end of hanging-wall of the YBF, which suggest **a3** transition (*solid line*) of movements along the YBF from mostly dip-slip in the south part to mostly strike-slip in the north; and graphs of cumulative relative frequency of distances from the transition line to every location and to landslide locations on **b1** the northern hanging-wall zone of the YBF and **b2** the southern hanging-wall zone of the YBF, which suggest **b3** three sub-zones with varying slips along the hanging-wall zone of the YBF

pattern of ETLs in relation to differences in slips along the hanging-wall of the YBF. The analyses for the three parts of the hanging-wall of the YBF show that the ETLs under study have positive spatial associations with the YBF (Fig. 7). However, the difference curves in Fig. 7 show that in the southern part, compared with the central and

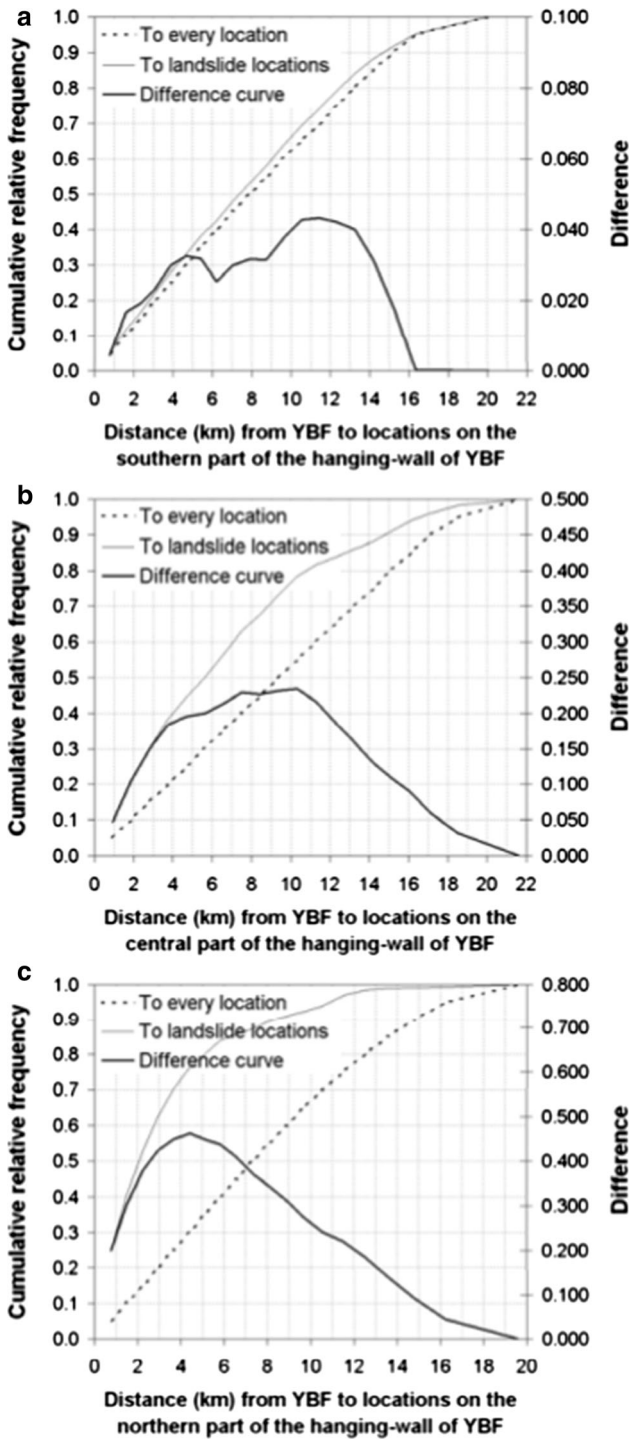

Fig. 7 Graphs of cumulative relative frequency of distances from the YBF to every location and to landslide locations on different parts of its hanging-wall zone (see Fig. 6b3): **a** southern part, **b** central part and **c** northern part

northern parts, of the hanging-wall of the YBF there is lowest likelihood of occurrence of ETLs due to proximity to the YBF than would be expected due to random chance. This result may seem odd in view of the fact that about 60 % of ETLs on the hanging-wall of the YBF are located in its 100-m-long southern part (cf. Fig. 6b2). However, we interpret this 'odd' result to mean that, in the southern hanging-wall of the YBF, there are other factors of earthquake-triggered landslide occurrence that are likely more important than proximity to the YBF, although, in the central and northern hanging-wall of the YBF, those factors are likely less important than proximity to the YBF. For example, because the south end of the hanging-wall of the YBF is about 15 km from the epicentre of the 2008 Wenchuan earthquake (see Figs. 2, 4 and 5), proximity to the earthquake epicentre rather than to the YBF is likely more important for earthquake-triggered landslide occurrence in the southern hanging-wall of the YBF but likely less important in the central and northern hanging-wall of the YBF. In addition, Precambrian crystalline and metamorphic rocks underlie the southern hanging-wall of the YBF, whereas Cambrian sedimentary rocks underlie the central and northern hanging-wall of the YBF, suggesting that lithology may have more influence on earthquake-triggered landslide occurrence in the southern hanging-wall of the YBF but less in the central and northern hanging-wall of the YBF. Moreover, slope failures in brittle rock are sensitive to high accelerations commonly within higher frequencies of ground motion (Jibson et al. 2006). However, Gorum et al. (2011) analysed the density of ETLs in two areas: one is homogeneously underlain by Precambrian crystalline rocks and the other by Cambrian sedimentary rocks. Each of these areas is located on the hanging-wall of the YBF with different fault geometries. Gorum et al. (2011) found that changes in lithology do not explain significant changes in the density of ETLs on the hanging-wall of the YBF. In addition, Ouimet (2009) stated also that variations in the spatial pattern of ETLs relative to different components of the surface rupture do not correspond to changes in lithology. Besides those independent findings in the study area, the analyses shown in Fig. 7b, c, which pertain to areas underlain by Cambrian sedimentary rocks, show different spatial patterns of ETLs. Thus, changes in underlying lithology do not seem to have an influence on the spatial pattern of ETLs in the study area, although this may not be the case in other areas.

Nevertheless, Fig. 7 further illustrates interesting features in relation to the second research question as describe below. The distance distribution analysis for the southern hanging-wall of the YBF shows three peaks along the difference curve, suggesting the presence of three populations of ETLs lying at, respectively, roughly 4.7, 8 and 11.5 km from the YBF (Fig. 7a). The distance distribution analysis for the central hanging-wall of the YBF shows three peaks along the difference curve, suggesting the presence of three populations of ETLs lying at, respectively, roughly 4.7, 7.5 and 10.3 km from the YBF

(Fig. 7b). The distance distribution analysis for the northern hanging-wall of the YBF shows a major peak and a subtle peak along the difference curve, suggesting the presence of two populations of ETLs lying at, respectively, roughly 4.4 and 11.5 km from the YBF (Fig. 7c). The similar maximum distances of spatial patterns of ETLs on the hanging-wall of the YBF (Fig. 7) are consistent with the findings of Yin et al. (2010) and Zhuang et al. (2010) about the widths of zones on the hanging-wall of the YBF with highest densities of ETLs (i.e. 11.5 and 15 km, respectively). However, the similar minimum and maximum distances of spatial pattern of ETLs on the hanging-wall of the YBF and the similar intermediate distances of spatial patterns of ETLs on the southern and central parts of that zone require interpretation.

The results of distance distribution analysis to examine the second research question can be interpreted in view of aspect ratios of asperities of surface ruptures associated with earthquake faults. An asperity is a zone along a fault surface that has a larger slip rate compared with the average slip rate along that fault, and its along-strike length to down-dip width ratio is called its aspect ratio. Somerville et al. (1999) observed that asperities of strike-slip earthquake faults are roughly 2× larger than asperities of dip-slip earthquake faults, which indicate that zones of strong ground motion associated with strike-slip earthquake faults are narrower than zones of strong ground motion associated with dip-slip earthquake faults. This is likely the case along the YBF in view of the changes in geometry of the different parts of this fault (Fig. 3) and variations in co-seismic slip distributions along this fault (Fig. 4). If that is the case, the results of distance distribution analysis can be interpreted as follows. Within the defined 21-km-wide zone on the hanging-wall of the YBF, ETLs lying 4.4–4.7 km from the YBF are likely associated with strike-slips, whereas ETLs lying 10.3–11.5 km from the YBF are likely associated with thrust-slips. Within the southern and central parts of the hanging-wall of the YBF, ETLs lying 7.5–8 km from the YBF are likely associated with oblique-slips having roughly equal thrust- and strike-slip components. These interpretations can be investigated further via the application of Fry analysis.

Fry analysis of landslide distribution

Fry points of ETLs on the southern hanging-wall of the YBF exhibit 30°–45° major trends, those on the central hanging-wall exhibit 0°–15° and 30°–45° major trends, and those on the northern hanging-wall exhibit 0°–15° and 60°–75° major trends (Fig. 8a). Fry points of ETLs on the hanging-wall of the PF, which has geometry and kinematics similar to YBF, exhibit major and minor trends that are closely similar to those on the southern hanging-wall of the YBF. The 30°–45° major trends exhibited by ETLs on the southern and central parts of the hanging-wall of the YBF follow the main strike of this fault and are likely associated with thrust-slips of the YBF. That is because HWs of major thrust (or reverse dip-slip) faults, such as the YBF, usually exhibit imbricate stacking of minor thrust faults that strike parallel to the main thrust fault (e.g. Lacombe et al. 1999). The 0°–15° and 60°–75° major trends exhibited by ETLs on the northern hanging-wall of the YBF are likely associated with strike-slips of the YBF. That is because a horizontal σ_1 oriented at 30°–45° (i.e. along the strike of YBF) and a horizontal σ_3 oriented perpendicular to σ_1 would result in Riedel shears or conjugate Riedel shears that strike 0°–15° and/or 60°–75° (Petit 1987). Accordingly, the 0°–15° major trends exhibited by ETLs on the central hanging-wall of the YBF are also likely associated with strike-slip components of oblique-slips of the YBF. Likewise, the 0°–15° and 60°–75° minor trends exhibited by ETLs on the southern hanging-wall of the YBF and the 60°–75° minor trends exhibited by ETLs on the central hanging-wall of the YBF (Fig. 8a) are likely associated with strike-slip components of oblique-slips of the YBF. In contrast, the 30°–45° minor trends exhibited by ETLs on the northern hanging-wall of the YBF are likely associated with minor thrust-slip components of oblique-slips of the YBF. The 150°–165° and 115°–120° minor trends exhibited by ETLs on, respectively, the central and northern hanging-wall of the YBF are possibly associated with minor normal-slip faults, which, although not reported in the hanging-wall of the YBF, are not rare in strike-slip fault systems. Thus, the Fry analyses illustrate that trends in the spatial patterns of ETLs on different parts of the hanging-wall of the YBF are consistent with general knowledge of fault kinematics. In the succeeding paragraphs, we describe results of Fry analyses, using ETLs located 0–15, 0–10 and 0–5 km west and in the 21-km-wide zone of hanging-wall of the YBF, to investigate further our earlier interpretations of the results of distance distribution analysis shown in Fig. 7.

For ETLs on the southern hanging-wall of the YBF, Fig. 8a–d shows consistency of 30°–45° major trends and gradual increase in frequency of 0°–15° trends from the western boundary of the southern hanging-wall of the YBF to the surface ruptures along the YBF. In particular, ETLs located 0–5 km west and on the southern hanging-wall of the YBF exhibit not only 30°–45° major trends but also 0°–15° major trends. These results and the inference that 0°–

Fig. 8 Rose diagrams of trends between pairs of 60-m spaced Fry points of earthquake-induced landslides **a** located on different parts of the hanging-wall zone of the YBF and on the hanging-wall zone of the Pengguan fault, **b** located 0–15 km from the YBF and on different parts of the hanging-wall zone of that fault, **c** located 0–10 km from the YBF and on different parts of the hanging-wall zone of that fault and **d** located 0–5 km from the YBF and on different parts of the hanging-wall zone of that fault. *Colours* of rose diagrams correspond to colour of hanging walls of the faults

15° trends are likely associated with strike-slips, albeit less predominant than thrust-slips, in the southern hanging-wall of the YBF, support our earlier interpretation that ETLs lying 4.4–4.7 km from the YBF are likely associated with strike-slips. The gradual decrease in frequency of 0°–15° minor trends from the surface ruptures along the YBF to the western boundary of the southern hanging-wall of the YBF also means gradual increase in frequency of 30°–45° major trends along the same direction. This result and the inference that 30°–45°.trends are likely associated with

thrust-slips in the southern hanging-wall of the YBF support our earlier interpretation that ETLs lying 10.3–11.5 km from the YBF are likely associated with thrust-slips. The consistency of 30°–45° major trends and the change from 0°–15° major trends to 0°–15° intermediate trends from the YBF up to 10 km towards the west (Fig. 8c, d) suggest increasing thrust-slip components of oblique-slips across the width of the southern hanging-wall of the YBF. This inference supports our earlier interpretation that ETLs lying 7.5–8 km from the YBF are likely associated with oblique-slips having thrust-slip components that more likely predominate over strike-slip components.

For ETLs on the central hanging-wall of the YBF, Fig. 8a–d shows consistency of 30°–45° major trends, minor fluctuations of 0°–15° major trends and subtle increase in frequency of 60°–75° minor trends from the western boundary of the central hanging-wall of the YBF to the surface ruptures along the YBF. These results and the inference that 60°–75° trends are likely associated with strike-slips in the central hanging-wall of the YBF support our earlier interpretation that ETLs lying 4.4–4.7 km from the YBF are likely associated with strike-slips. The minor fluctuations of 0°–15° major trends and the subtle decrease in frequency of 60°–75° minor trends from the surface ruptures along the YBF to the western boundary of the central hanging-wall of the YBF (Fig. 8a–d) also mean subtle increase in frequency of 30°–45° major trends along the same direction. This result and the inference that 30°–45° trends are likely associated with thrust-slips in the central hanging-wall of the YBF support our earlier interpretation that ETLs lying 10.3–11.5 km from the YBF are likely associated with thrust-slips. The consistency of 30°–45° major trends and the subtle decrease in frequency of 60°–75° minor trends from the YBF up to 10 km towards the west (Fig. 8c, d) suggest increasing thrust-slip components of oblique-slips across the width of the central hanging-wall of the YBF. This inference supports our earlier interpretation that ETLs lying 7.5–8 km from the YBF are likely associated with oblique-slips having more or less equal thrust- and strike-slip components.

For ETLs on the northern hanging-wall of the YBF, Fig. 8a–d shows minor fluctuations of 0°–15° and 60°–75° major trends and subtle decrease in frequency of 30°–45° minor trends from the western boundary of the northern hanging-wall of the YBF to the surface ruptures along the YBF. These results and the inference that 30°–45° trends are likely associated with thrust-slips in the northern hanging-wall of the YBF support our earlier interpretation that ETLs lying 10.3–11.5 km from the YBF are likely associated with thrust-slips. The subtle increase in frequency of 30°–45° minor trends from the surface ruptures along the YBF to the western boundary of the northern hanging-wall of the YBF also means subtle decrease in frequency of 0°–15° and 60°–75° major trends along the same direction. This result and the inference that 0°–15° and 60°–75° major trends are likely associated with strike-slips in the northern hanging-wall of the YBF support our earlier interpretation that ETLs lying 4.4–4.7 km from the YBF are likely associated with strike-slips.

Representation of fault control on susceptibility to landsliding

We applied data-driven estimation of EBFs to create a predictor map representing fault controls on susceptibility to occurrence of ETLs. We used distances from the YBF to locations in the same 240-km-long and 21-km-wide zone of the hanging-wall of the YBF so that the results were directly comparable to the analyses described in the preceding sections. Our aim here was not to derive a predictive map of susceptibility to occurrence of ETLs for policy decision-making, so we did not create and integrate predictor maps representing other spatial controls on this phenomenon. However, a predictor map is by itself a predictive map. Thus, its predictive capacity can be evaluated. To do so, we divided the same set of ETLs used in the preceding analyses into two subsets with equal number of ETLs and roughly the same spatial pattern. We achieved that by adding a dummy variable in our database and then labelling the ETLs alternately with '1' and '2'. Earthquake-triggered landslides labelled '1' comprised one subset and those labelled '2' comprised the other subset. One subset (called training subset) of ETLs was used for estimating EBFs and creating a predictor map, whereas the other subset (called validation subset) was used for evaluating the prediction accuracy of a predictor map. The roles of both subsets of ETLs were then reversed for cross-checking of results. We performed these analyses to support our proposition that using classified faults, rather than using unclassified faults, provides for proper spatial representation of fault control as a predictor of susceptibility to occurrence of ETLs.

By classifying parts of the YBF according to style-of-faulting based on the analyses described in the preceding sections, we estimated EBFs of classes of 5-percentile interval distances from the YBF in each part of the hanging-wall of this fault. Assuming that parts of the YBF are unclassified according to style-of-faulting, we estimated EBFs of classes of 5-percentile interval distances from the YBF in the 240-km-long and 21-km-wide zone of the

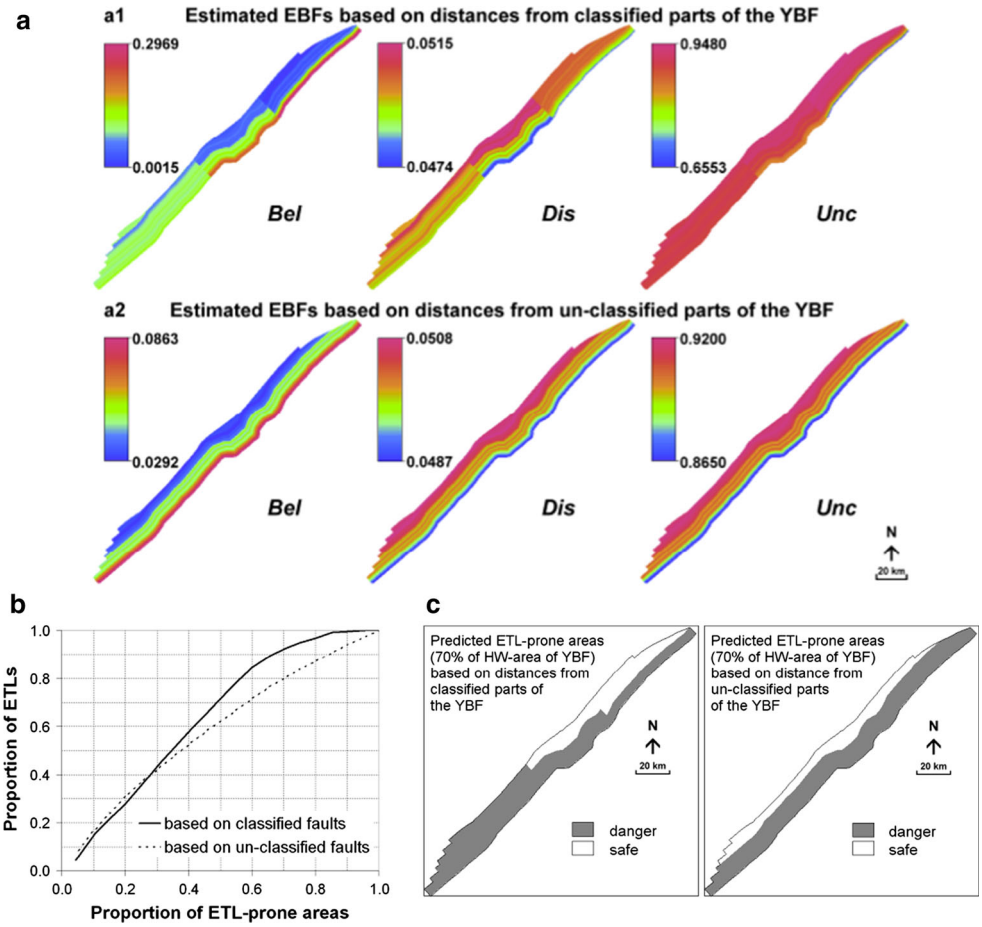

Fig. 9 Results of representation of style-of-faulting controls on susceptibility to landsliding. **a** Estimates of evidential belief functions (*Bel* belief, *Dis* disbelief, *Unc* uncertainty) based on distances from classified and unclassified parts of the YBF with respect to earthquake-induced landslide occurrence. **b** Prediction accuracy curves of maps of *Bel* obtained by using distance from classified and unclassified parts of the YBF as predictor. **c** Binary maps of predicted ETL-prone zones based on maps of *Bel* obtained by using distance from classified and unclassified parts of the YBF as predictor

hanging-wall of the YBF. If parts of the YBF are classified according to style-of-faulting, values of EBFs with respect to ETLs vary depending on style-of-faulting (Fig. 9a). The estimated values of *Bel* suggest that in the southern hanging-wall of the YBF the likelihood of occurrence of ETLs is the lowest, in the central hanging-wall of the YBF intermediate and in the northern hanging-wall of the YBF the highest. This is consistent with what the difference curves in Fig. 7 suggest as discussed earlier. In contrast, if parts of the YBF are unclassified, values of EBFs increase monotonously with increasing distance from the YBF (Fig. 9a). Variations in values of *Bel* suggest that areas closest to and farthest from the YBF have, respectively, highest and lowest susceptibility to earthquake-triggered landslide occurrence (Fig. 9a). A simple visual comparison of the patterns of variations in estimated EBFs (Fig. 9a) with the spatial pattern of ETLs (Fig. 2) suggests that using classified faults results in better spatial representation of fault control on susceptibility to earthquake-triggered landslide occurrence.

We applied the technique described by Chung and Fabbri (1999) to evaluate the prediction accuracy of a map of *Bel* against a validation subset. Cumulative decreasing values of *Bel* define cumulative increasing proportions of ETL-prone areas, from which cumulative increasing proportions of ETLs in the validation subset can be determined (Fig. 9b). Proportions of ETLs in a validation subset delineated in ETL-prone areas define the prediction accuracy of a predictor map. If areas covering $\leq$30 % of the 240-km-long and 21-km-wide zone of the hanging-wall of the YBF are considered ETL-prone according to certain cut-off values of *Bel*, there is minimal difference in using classified or unclassified faults (Fig. 9b). However, if areas covering >30 % of the 240-km-long and 21-km-wide zone of the hanging-wall of the YBF are considered ETL-prone according to certain cut-off values of *Bel*, the prediction accuracy curve obtained using classified faults is above the prediction accuracy curve obtained using un-classified faults. This illustrates the benefit of classifying faults according to style-of-faulting as explained further below.

Let us assume that a prediction of 70 % ETL-prone zones in the hanging-wall of the YBF is correct (Fig. 9c). On the one hand, when distance from unclassified parts of the YBF is used as predictor, the prediction accuracy corresponding to a prediction of 70 % ETL-prone zones is 80 % (Fig. 9b). The same prediction accuracy can be achieved when distance from classified parts of the YBF is used as predictor, but the predicted ETL-prone zones would be 14 % less. Thus, a prediction of 14 % more ETL-prone zones would constitute a *false-positive* error if we use distance from classified parts of the YBF as predictor. Visual comparison of the predicted ETL-prone zones (Fig. 9c) with the spatial pattern of ETLs (Fig. 2) suggests that the false-positive error obtained by using distance from classified parts of the YBF as predictor pertains mainly to the central parts of the hanging-wall of the YBF. On the other hand, when distance from classified parts of the YBF is used as predictor, the prediction accuracy corresponding to a prediction of 70 % ETL-prone zones is 93 % (Fig. 9b). The same prediction accuracy can be achieved when distance from unclassified parts of the YBF is used as predictor, but the predicted ETL-prone zones would be 18 % more. Thus, a prediction of 18 % more ETL-prone zones would constitute a *false-negative* error if we use distance from un-classified parts of the YBF as predictor. Visual comparison of the predicted ETL-prone zones (Fig. 9c) with the spatial pattern of ETLs (Fig. 2) suggests that the false-negative prediction error obtained by using distance from unclassified parts of the YBF as predictor pertains mainly to the southern parts of the hanging-wall of the YBF.

In statistical hypothesis testing, false-positive and false-negative errors are called Type I and Type II errors, respectively. In evaluating predictive maps of Nat Hazards, Type I error represents overestimation of hazard, whereas Type II error represents underestimation of hazard (Begueria 2006). It is desirable to have both minimal Type I and Type II errors. It is, however, more desirable to have Type II error lower than Type I error, because it is conceivable that gross underestimation (false-negative error) of landslide hazard, rather than gross overestimation (false-positive error) of landslide hazard, could potentially result in higher damage to lives and properties. Thus, based on the prediction accuracy curves (Fig. 9b) and visual comparison of the predicted ETL-prone zones (Fig. 9c) with the spatial pattern of ETLs (Fig. 5), we can say that using classified faults, rather than using unclassified faults, provides for better spatial representation of fault control as a predictor of susceptibility to occurrence of ETLs.

Overall discussion of results

Earthquake-triggered landslides are without doubt associated with faults, earthquake faults specifically. However, studies dealing with effects of long-term regional or local deformations, associated with tectonic movements, on landslide formation in a geomorphologic perspective are prolific in the literature (e.g. Alexander and Formichi 1993; Guzzetti et al. 1996; Gupta 2005; Korup et al. 2007, 2010; Ghosh et al. 2010), but there is a paucity of studies on the influence of style-of-faulting on mass wasting processes such as landsliding. Nevertheless, the above-mentioned studies commonly suggest that (1) the effects of tectonics on landslide occurrence differ according to the characteristics (quantity, magnitude, style, etc.) of long-term deformations in any particular region and (2) directions of tectonic stresses significantly control the distribution of landslides. Accordingly, while the principal stress axis in a region determines geometry and style-of-faulting, it also influences, in the long-term, variations in orientations and distributions of landforms and relationships among geomorphic systems. Therefore, although the above-mentioned studies generally focus on the formative effects of landslides in tectonic-dominated landscapes or mountain belts, they implicitly point out that faults or fractures, depending on the characteristics of deformation, influence selective erosion processes and control the occurrence, density and distribution of landslides.

There is, however, a paucity of published studies (at least in English journals) about the relationship between the spatial pattern of ETLs and style-of-faulting. One likely reason for that is most earthquake faults were ‘single-slip’ (dextral, sinistral, normal, reverse or thrust) and some were oblique-slip. For example, among the 224 earthquake faults listed in Wells and Coppersmith (1994), which occurred between 1856 and 1993, 75 % were single-slip and 25 % were oblique-slip. In addition, the following earthquakes that occurred in the last decade and triggered landslides were also mainly either reverse- or thrust-slip: 1999 Chi–Chi earthquake, Taiwan (Huang et al. 2001; Shou and Wang 2003; Khazai and Sitar 2004; Chang et al. 2005); 2002 Avaj earthquake, Iran (Mahdavifar et al. 2006); 2004 Niigata Ken Chuetsu earthquake, Japan (Sato et al. 2005; Chigira and Yagi 2006; Kieffer et al. 2006; Wang et al. 2008a, b); and 2005 Kashmir earthquake, Pakistan (Owen et al. 2008). The 2002 earthquake in Alaska that triggered landslides was associated with the Denali fault, which is one of the longest strike-slip systems in the world (Jibson et al. 2006), although during the earthquake slips along the

fault rupture were oblique-slips with predominant strike-slip components (Frankel et al. 2002; Dreger et al. 2004; Velasco et al. 2004). Nevertheless, several other factors influence the spatial pattern of ETLs around earthquake faults (e.g. see references cited in the second paragraph of the Introduction). Thus, in spite of the disaster brought about by the 2008 Wenchuan earthquake, the associated Yingxiu–Beichuan fault, which had mainly thrust-slips in the south to mainly dextral strike-slips in the north, provided the opportunity to examine the spatial pattern of ETLs with respect to style-of-faulting.

To examine the spatial pattern of ETLs with respect to style-of-faulting, we had to adapt the co-seismic rupture boundary defined by Shen et al. (2009) on the hanging-wall of the Yingxiu–Beichuan fault as a reference area (Fig. 5). This strategy of using a reference area to analyse the spatial pattern of landslides triggered by that earthquake was demonstrated by Keefer (2000). The logic of studying the distribution of ETLs on the hanging-wall of faults is based on findings that, during earthquakes, ground motions are stronger on the hanging-wall than on the footwall of a dipping earthquake fault (Abrahamson and Somerville 1996; Yu and Gao 2001; Ulusay et al. 2004). The proposed explanation for those observations is asymmetry of distribution of seismic energy as a function of fault geometry (Oglesby and Day 2002; Beavan et al. 2012; Shi and Day 2013; Gabuchian et al. 2014), although that is usually not the case because attenuation of ground motion is also a function of style-of-faulting (Campbell 1981; Abrahamson and Silva 1997; Bommer et al. 2003). Nevertheless, studies have shown that ground motions on the hanging wall were stronger than on the footwall of the Yingxiu–Beichuan fault (Zhang et al. 2008; Lu et al. 2010). Thus, using the co-seismic rupture boundary defined by Shen et al. (2009) on the hanging-wall of the Yingxiu–Beichuan fault as a reference area is justified in our study.

As stated earlier in "Distance distribution analysis of landslide distribution" section, the traditional way of describing the spatial pattern of landslides by counting the number or calculating the percentage of landslides (depicted as points) per square kilometre of reference area is inadequate for examining control of style of earthquake faults on the spatial pattern of ETLs. Therefore, we applied the distance distribution analysis (Berman 1977, 1986) for quantifying spatial dependence of a point process on another stochastic process. This method has only been used recently by Ghosh and Carranza (2010) to study landslide controls, but it has been employed extensively in studies of mineralization controls (e.g. Bonham-Carter 1985; Carranza and Hale 2002; Carranza et al. 2008a). In the present study, we applied distance distribution analysis not only because it is a probabilistic method but also because (a) distance to fault is suitable for ground motion attenuation analysis (Campbell 1981, 1997), (b) variations in ground motion are influenced by the style of earthquake faults (Campbell 1981; Bommer et al. 2003) and (c) ground motion is a factor of ETLs (Jibson and Keefer 1993; Miles and Ho 1999). To support the results of distance distribution analysis, we applied Fry analysis (Fry 1979) for investigating strain and strain partitioning in rocks. Likewise, Fry analysis has only been used recently by Ghosh and Carranza (2010) to study landslide controls, but it has been employed extensively to deduce trends of structures controlling mineralization (e.g. Vearncombe and Vearncombe 1999; Carranza 2009, 2011; Carranza et al. 2009; Carranza and Sadeghi 2010) and geothermal fields (Carranza et al. 2008b) as well as to infer post-mineralization deformation (Carranza and Sadeghi 2014). As shown by Ghosh and Carranza (2010), distance distribution analysis and Fry analysis are complementary and supplementary methods that can be used in conjunction with one another to investigate certain controls on landsliding. Distance distribution analysis is useful in determining optimum range of distance between ETLs and a fault (or a set of faults), which indicates that the former are spatially dependent on the latter. Fry analysis is useful in determining trends in the spatial pattern of ETLs, which allow deduction of style-of-faulting. We also show this here by revisiting to summarize the results of analyses with regard to the two research questions brought out in the Introduction.

Regarding the first research question, the distance distribution analyses (Figs. 6, 7) suggest that the spatial pattern of ETLs allows partitioning of a fault in terms of predominant style-of-faulting. Of course, we have a priori knowledge of variations in style-of-faulting along the Yingxiu–Beichuan fault, which may have led us to interpret the results as such. This illustrates, however, the importance of mapping and classification of faults, active faults in particular, in tectonically mobile belts or regions of high seismicity where earthquakes frequently occur. Granted that a priori knowledge of style-of-faulting and co-seismic fault plane boundary are lacking, we can still examine the spatial pattern of ETLs to determine whether a mapped but unclassified fault can be partitioned according to predominant style-of-faulting along that fault. To do so, distance distribution analysis must be performed on either side of that fault by using a reference area that extends in a direction perpendicular to that fault and covers all earthquake-triggered on one side that fault. As example, Fig. 10

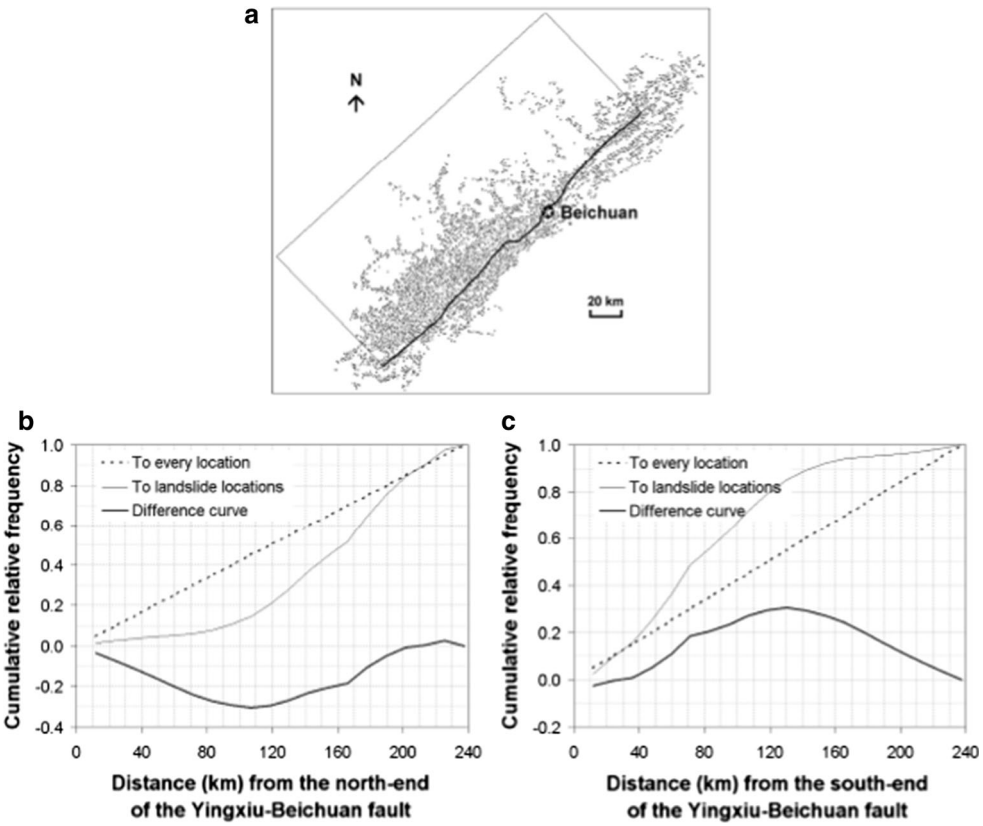

Fig. 10 Analysis of spatial pattern of earthquake-induced landslides in an area west of the YBF. See text for discussion

shows results for the west side of the Yingxiu–Beichuan fault that are similar to those shown in Fig. 6. Therefore, if we proceed further with the same analyses described in "Distance distribution analysis of landslide distribution" section and shown in Fig. 6, and if we synthesize results from each side of the fault, we would likely reach similar interpretations about where to partition a fault in terms only of plausible predominant style-of-faulting based on variations in the spatial patterns of ETLs. To support such interpretations, we have to perform distance distribution analysis for different parts of a fault as described in "Distance distribution analysis of landslide distribution" section and shown in Fig. 7.

Note, however, that the distance distribution analyses shown in Figs. 6 and 7 describe the spatial pattern of ETLs with respect to not only style-of-faulting but also distance from epicentre. For the analyses shown in Fig. 10, we may assume lack of a priori knowledge of epicentre location such that we have less argument for partitioning a fault in terms of plausible predominant style-of-faulting based on variations in the spatial patterns of ETLs. Nevertheless, if we were to perform Fry analysis for the same parts of that fault, as described earlier in "Fry analysis of landslide distribution" section and shown in Fig. 8a–d, we would likely obtain trends in the spatial pattern of ETLs that are likely associated with style-of-faulting as discussed above. Thus, to examine the spatial pattern of ETLs with respect to style-of-faulting, distance distribution analysis and Fry analysis must be applied in conjunction with each other rather than to apply just one of them.

Regarding the second research question, the results of distance distribution analyses shown in Fig. 7 and the results of Fry analyses shown in Fig. 8a–d suggest that the spatial pattern of ETLs varies with respect to the predominant style-of-faulting. The results, as discussed earlier in "Distance distribution analysis of landslide distribution" and "Fry analysis of landslide distribution" sections, suggest that ETLs associated with thrust-slips mostly occur farther away from the earthquake fault, whereas ETLs associated with strike-slips mostly occur closer to the earthquake fault. These findings cohere with the knowledge that attenuation of ground motion is a function of style-of-faulting (Campbell 1981; Abrahamson and Silva 1997; Bommer et al. 2003). However, the findings must be cross-examined further in relation to fault geometry because (a) the mainly thrust-slip southern part of the Yingxiu–Beichuan fault has a different geometry than its mainly strike-slip northern part (Fig. 3) and (b) attenuation of

ground motion is also a function of fault geometry (Oglesby and Day 2002; Beavan et al. 2012; Shi and Day 2013; Gabuchian et al. 2014). In addition, the findings must be cross-examined further in relation to other factors that influence variations in ground motion (see Campbell (1981, 1997)). Nevertheless, the results of analyses support our hypothesis that the spatial pattern of ETLs is influenced by style-of-faulting. In addition, we have shown in "Representation of fault control on susceptibility to landsliding" section that using classified faults, rather than using unclassified faults, provides for better spatial representation of fault control as a predictor of susceptibility to occurrence of ETLs.

If we were to choose an area for cross-comparing our findings for the hypothesis that we have examined, we would chose the area wherein the 3 November 2002 M_w 7.9 Alaska earthquake occurred. The reasons for this choice are: (a) the terrain characteristics of that area are similar to those in the Wenchuan area; (b) that earthquake has the same magnitude as the 12 May 2008 Wenchuan earthquake; (c) the 300-km-long rupture generated along the Denali fault by that earthquake is, on a regional-scale, similar to the 240-km-long rupture generated along the Yingxiu–Beichuan fault by the 12 May 2008 Wenchuan earthquake; and (d) the landslides triggered by that earthquake were concentrated mostly in a roughly 30-km-wide zone around the surface rupture (Eberhart-Phillips et al. 2003; Jibson et al. 2006). However, compared with tens of thousands of landslides triggered by the 2008 Wenchuan earthquake, only thousands of landslides were triggered by the 2002 Alaska earthquake (Harp et al. 2003; Jibson et al. 2004, 2006; Kayen et al. 2004). In addition, unlike the variable slips along the Yingxiu–Beichuan fault during the 12 May 2008 Wenchuan earthquake, the slips along the Denali fault during the 3 November 2002 were oblique with predominant strike-slip components (Frankel et al. 2002; Dreger et al. 2004; Velasco et al. 2004). We believe that these similarities and differences between surface ruptures and associated landslides linked to the 2002 Alaska and 2008 Wenchuan earthquakes are instructive in increasing our understanding of the relationship between spatial patterns of ETLs and styles of earthquake faults. In turn, better understanding of that relationship is essential for proper spatial representation of landslide controls in predictive modelling of areas susceptible to earthquake-triggered landsliding.

Predictive modelling of areas susceptible to occurrence of ETLs (or landslides triggered by other phenomenon) can be categorized into two types—mechanistic and empirical (Harbaugh and Bonham-Carter 1970). On the one hand, mechanistic modelling applies fundamental or theoretical knowledge of processes and their interactions to predict or understand the system of interest. Examples of mechanistic modelling of susceptibility to occurrence of ETLs are those that apply Newmark's (1965) sliding block or displacement method (e.g. Wilson and Keefer 1985; Miles and Ho 1999; Wu et al. 2009; Wang and Lin 2010; Wu and Tsai 2011). The Newmark analysis, which is suitable for site-specific modelling of seismic hazard as applied in California for seismic safety (CGS 2008), makes use of peak ground acceleration data related not to style-of-faulting but to earthquake epicentre location and slope. On the other hand, empirical modelling characterizes or quantifies the influence of one or more underlying processes, which are known insufficiently or indirectly, on the behaviour of the system of interest. Examples of empirical modelling of susceptibility to occurrence of ETLs, such as those cited in the first paragraph of the Introduction (e.g. Jaafari et al. 2014; Pourghasemi et al. 2014; Regmi et al. 2014), are data driven, meaning that they are based on empirical analysis of spatial relationships between occurrences of ETLs and various spatial factors. In contrast, Miles and Keefer (2007) developed CAMEL (comprehensive areal model of earthquake-triggered landslides) for knowledge-driven regional-scale empirical analysis in a GIS. Miles and Keefer (2009) further developed CAMEL to allow integration of Newmark's (1965) displacement model. Although our present study involves data-driven empirical spatial analysis, the new knowledge gained from the analyses of spatial pattern of ETLs with respect to style-of-faulting in the Wenchuan area is likely to be beneficial in the application of CAMEL. In addition, the knowledge that the spatial pattern of ETLs is influenced by style-of-faulting bears the importance of mapping and classification of faults in predictive mapping of susceptibility to occurrence of not only ETLs but also other types of structurally controlled landslides.

Conclusion

The salient conclusions that can be drawn from the present study are the following. The Yingxiu–Beichuan fault rupture and the tens of thousands of landslides that were associated with the 2008 Wenchuan earthquake provided the opportunity to carry out the study because the style-of-faulting along that fault, from its southern to northern parts, varied from mainly thrust-slip to mainly strike-slip. Distance distribution analysis and Fry analysis are complementary and supplementary methods that can be used in conjunction with one another to study the spatial pattern of earthquake-triggered landslides in relation to style-of-

faulting. Analysis of the spatial pattern of earthquake-triggered landslides allows classification of segments of the associated earthquake fault in terms of predominant style-of-faulting. The spatial patterns of earthquake-triggered landslides vary with respect to predominant style-of-faulting along the earthquake fault. On the hanging-wall of Yingxiu–Beichuan fault, earthquake-triggered landslides lying mostly at 10.3–11.5 km from the fault are likely associated with thrust-slips, earthquake-triggered landslides lying mostly at 7.5–8 km from the fault are likely associated with oblique-slips, and earthquake-triggered landslides lying mostly at 4.4–4.7 km from the fault are likely associated with strike-slips. Therefore, earthquake-triggered landslides associated with thrust-slips mostly occur farther away from the earthquake fault, whereas earthquake-triggered landslides associated with strike-slips mostly occur closer to the earthquake fault. Classification of faults according to style-of-faulting is crucial in predictive mapping of susceptibility to occurrence of earthquake-triggered landslides. The spatial pattern of earthquake-triggered landslides is influenced by style-of-faulting. This proposition requires further examination in other areas. Further studies are needed to cross-examine the findings here in relation to fault geometry and other factors that influence variations in ground motions associated with earthquake faults.

Acknowledgments The first author thanks Cees J. van Westen for his encouragement and giving the opportunity to work in Longmen Shan region after the 12 May 2008 Wenchuan earthquake. He thanks also Run Qiu Huang and Qiang Xu of the State Key Laboratory of Geo-hazards Prevention and Geo-environment Protection, Chengdu University of Technology, for their support and kind hospitality during fieldwork. This research was financially supported by the National Basic Research Program '973' Project of the Ministry of Science and Technology of the People's Republic of China (2008CB425801) and by the United Nations University—ITC School for Disaster Geo-Information Management (www.itc.nl/unu/dgim).

References

Abrahamson NA, Silva WJ (1997) Empirical response spectral attenuation relations for shallow crustal earthquakes. Seismol Res Lett 68:94–127

Abrahamson NA, Somerville PG (1996) Effects of the hanging wall and footwall on ground motions recorded during the Northridge earthquake. Bull Seismol Soc Am 86:S93–S99

Alexander D, Formichi R (1993) Tectonic causes of landslides. Earth Surf Proc Land 18:311–338

Bai SB, Wang J, Thiebes B, Cheng C, Chang ZY (2014) Susceptibility assessments of the Wenchuan earthquake-triggered landslides in Longnan using logistic regression. Environ Earth Sci 71:731–743

Beavan J, Motagh M, Fielding EJ, Donnelly N, Collett D (2012) Fault slip models of the 2010–2011 Canterbury, New Zealand, earthquakes from geodetic data and observations of postseismic ground deformation. New Zeal J Geol Geophys 55:207–221

Begueria S (2006) Validation and evaluation of predictive models in hazard assessment and risk management. Nat Hazards 37:315–329

Berman M (1977) Distance distributions associated with Poisson processes of geometric figures. J Appl Probab 14:195–199

Berman M (1986) Testing for spatial association between a point processes and another stochastic process. Appl Stat 35:54–62

Bommer JJ, Douglas J, Stasser FO (2003) Style-of-faulting in ground-motion prediction equations. Bull Earthq Eng 1:171–203

Bonham-Carter GF (1985) Statistical association of gold occurrences with Landsat-derived lineaments, Timmins-Kirkland Lake area, Ontario. Can J Remote Sens 11:195–211

Boots BN, Getis A (1988) Point pattern analysis. Sage University Scientific Geography Series No. 8. Sage, Beverly Hills

Bradley BA, Quigley MC, Van Dissen RJ, Litchfield NJ (2014) Ground motion and seismic source aspects of the Canterbury earthquake sequence. Earthq Spectra 30:1–15

Burchfiel BC, Chen Z, Liu Y, Royden LH (1995) Tectonics of the Longmen Shan and adjacent regions, central China. Int Geol Rev 37:661–735

Campbell KW (1981) Near-source attenuation of peak horizontal acceleration. Bull Seismol Soc Am 71:2039–2070

Campbell KW (1997) Empirical near-source attenuation relationships for horizontal and vertical components of peak ground acceleration, peak ground velocity, and pseudo-absolute acceleration response spectra. Seismol Res Lett 68:154–179

Carranza EJM (2009) Controls on mineral deposit occurrence inferred from analysis of their spatial pattern and spatial association with geological features. Ore Geol Rev 35:383–400

Carranza EJM (2011) From predictive mapping of mineral prospectivity to quantitative estimation of number of undiscovered prospects. Resour Geol 61:30–51

Carranza EJM, Castro OT (2006) Predicting lahar-inundation zones: case study in West Mount Pinatubo, Philippines. Nat Hazards 37:331–372

Carranza EJM, Hale M (2002) Spatial association of mineral occurrences and curvilinear geological features. Math Geol 34:199–217

Carranza EJM, Hale M (2003) Evidential belief functions for geologically constrained mapping of gold potential, Baguio district, Philippines. Ore Geol Rev 22:117–132

Carranza EJM, Sadeghi M (2010) Predictive mapping of prospectivity and quantitative estimation of undiscovered VMS deposits in Skellefte district (Sweden). Ore Geol Rev 38:219–241

Carranza EJM, Sadeghi M (2014) Post-VMS mineralization deformations (1.88–1.82 Ga) of the Skellefte district (Sweden): insights from the spatial pattern of VMS occurrences. Front Earth Sci 8:319–324

Carranza EJM, Hale M, Faassen C (2008a) Selection of coherent deposit-type locations and their application in data-driven mineral prospectivity mapping. Ore Geol Rev 33:536–558

Carranza EJM, Wibowo H, Barritt SD, Sumintadireja P (2008b) Spatial data analysis and integration for regional-scale geothermal potential mapping, West Java, Indonesia. Geothermics 33:267–299

Carranza EJM, Owusu EA, Hale M (2009) Mapping of prospectivity and estimation of number of undiscovered prospects for lode-gold, southwestern Ashanti Belt, Ghana. Min Deposita 44:915–938

CGS (2008) Guidelines for evaluating and mitigating seismic hazards in California. Special Publication 117A. California Geological Survey (CGS), Sacramento

Chang J, Slaymaker O (2002) Frequency and spatial distribution of landslides in a mountainous drainage basin: western foothills, Taiwan. Catena 46:285–307

Chang KJ, Taboada A, Chan YC (2005) Geological and morphological study of the Jiufengershan landslide triggered by the Chi–Chi Taiwan earthquake. Geomorphology 71:293–309

Chen XL, Zhou Q, Ran H, Dong R (2012) Earthquake-triggered landslides in southwest China. Nat Hazards Earth Syst Sci 12:351–363

Chernoff H, Lehmann EL (1954) The use of maximum likelihood estimates in χ^2 tests for goodness-of-fit. Ann Math Stat 25:579–586

Chigira M, Yagi H (2006) Geological and geomorphological characteristics of landslides triggered by the 2004 Mid Niigata prefecture earthquake in Japan. Eng Geol 82:202–221

Chigira M, Wu X, Inokuchi T, Wang G (2010) Landslides induced by the 2008 Wenchuan earthquake, Sichuan, China. Geomorphology 118:225–238

Chung CJF, Fabbri AG (1999) Probabilistic prediction models for landslide hazard mapping. Photogramm Eng Rem Sens 65:1389–1399

Crozier MJ, Deimel MS, Simon JS (1995) Investigation of earthquake triggering for deep-seated landslides, Taranaki, New Zealand. Quatern Int 25:65–73

Dai FC, Xu C, Yao X, Xu L, Tu XB, Gong QM (2011) Spatial distribution of landslides triggered by the 2008 Ms 8.0 Wenchuan earthquake, China. J Asian Earth Sci 40:883–895

Das HO, Sonmez H, Gokceoglu C, Nefeslioglu HA (2013) Influence of seismic acceleration on landslide susceptibility maps: a case study from NE Turkey. Landslides 10:433–454

Dempster AP (1967) Upper and lower probabilities induced by a multivalued mapping. Ann Math Stat 38:325–339

Densmore AL, Ellis MA, Li Y, Zhou R, Hancock GS, Richardson NJ (2007) Active tectonics of the Beichuan and Pengguan faults at the eastern margin of the Tibetan Plateau. Tectonics 26:TC4005. doi:10.1029/2006TC001987

Dreger D, Oglesby D, Harris R, Ratchkovski N, Hansen R (2004) Kinematic and dynamic rupture models of the November 3, 2002 Mw 7.9 Denali, Alaska, earthquake. Geophys Res Lett. doi:10.1029/2003GL018333

Eberhart-Phillips D, Haeussler PJ, Freymueller JT, Frankel AD, Rubin CM, Craw P, Ratchkovski NA, Anderson G, Carver GA, Crone AJ, Dawson TE, Fletcher H, Hansen R, Harp EL, Harris RA, Hill DP, Hreinsdóttir S, Jibson RW, Jones LM, Kayen R, Keefer DK, Larsen CF, Moran SC, Personius SF, Plafker G, Sherrod B, Sieh K, Sitar N, Wallace WK (2003) The 2002 Denali Fault earthquake, Alaska: a large magnitude, slip-partitioned event. Science 300:1113–1118

Frankel AD, Biswas NN, Martirosyan AH, Dutt U, McNamara DE (2002) Rupture process of the M 7.9 Denali Fault, Alaska, earthquake determined from strong-motion recordings. EOS Trans Am Geophys Union 47:1340

Fry N (1979) Random point distributions and strain measurement in rocks. Tectonophysics 60:89–105

Fu B, Shi P, Guo H, Okuyama S, Ninomiya Y, Wright S (2011) Surface deformation related to the 2008 Wenchuan earthquake, and mountain building of the Longmen Shan, eastern Tibetan Plateau. J Asian Earth Sci 40:805–824

Gabuchian V, Rosakis AJ, Lapusta N, Oglesby DD (2014) Experimental investigation of strong ground motion due to thrust fault earthquakes. J Geophys Res Sol Ea 119:1316–1336

Ghosh S, Carranza EJM (2010) Spatial analysis of mutual faults/fracture and slope controls on rocksliding in Darjeeling Himalaya, India. Geomorphology 122:1–24

Ghosh S, Günther A, Carranza EJM, van Westen CJ, Jetten VG (2010) Rock slope instability assessment using spatially distributed structural orientation data in Darjeeling Himalaya (India). Earth Surf Proc Land 35:1773–1792

Gorum T, Fan X, van Westen CJ, Huang RQ, Xu Q, Tang C, Wang G (2011) Distribution pattern of earthquake-induced landslides triggered by the 12 May 2008 Wenchuan earthquake. Geomorphology 133:152–167

Gorum T, Korup O, Van Westen CJ, Van der Meijde M, Xu C, Van der Meer FD (2014) Why so few? Landslides triggered by the 2002 Denali earthquake, Alaska. Quatern Sci Rev 95:80–94

Gupta V (2005) The relationship between tectonic stresses, joint patterns and landslides in the higher Indian Himalaya. J Nepal Geol Soc 31:51–58

Guzzetti F, Cardinali M, Reichenbach P (1996) The influence of structural setting and lithology on landslide type and pattern. Environ Eng Geosci 2:531–555

Hanna SS, Fry N (1979) A comparison of methods of strain determination in rocks from southwest Dyfed (Pembrokeshire) and adjacent areas. J Struct Geol 1:155–162

Hao KX, Si HJ, Fujiwara H, Ozawa T (2009) Coseismic surface ruptures and crustal deformations of the 2008 Wenchuan earthquake Mw 7.9, China. Geophys Res Lett 36:L11303. doi:10.1029/2009GL037971

Harbaugh JW, Bonham-Carter GF (1970) Computer simulation in geology. Wiley-Interscience, New York

Harp EL, Jibson RW, Kayen RE, Keefer DK, Sherrod BL, Carver GA, Collins BD, Moss RES, Sitar N (2003) Landslides and liquefaction triggered by the M 7.9 Denali Fault earthquake of 3 November 2002. GSA Today 13:4–10

Hewitt K (1983) Seismic risk and mountain environments: the role of surface conditions in earthquake disaster. Mt Res Dev 3:27–44

Holzer TL (1994) Loma Prieta damage largely attributed to enhanced ground shaking. EOS Trans Am Geophys Union 75:299–301

Huang R, Fan X (2013) The landslide story. Nat Geosci 6:325–326

Huang R, Li W (2009) Analysis of the geo-hazards triggered by the 12 May 2008 Wenchuan earthquake, China. Bull Eng Geol Environ 68:363–371

Huang CC, Lee YH, Liu HP, Keefer DK, Jibson RW (2001) Influence of surface-normal ground acceleration on the initiation of the Jih-Feng-Erh-Shan landslide during the 1999 Chi–Chi, Taiwan, earthquake. Bull Seismol Soc Am 91:953–958

Huang R, Pei X, Fan X, Zhang W, Li S, Li B (2012) The characteristics and failure mechanism of the largest landslide triggered by the Wenchuan earthquake, May 12, 2008, China. Landslides 9:131–142

Huang Y, Yu M, Bhattacharya S (2014) Characteristics of flow failures triggered by recent earthquakes in China. Indian Geotech J 44:218–224

Jaafari A, Najafi A, Pourghasemi HR, Rezaeian J, Sattarian A (2014) GIS-based frequency ratio and index of entropy models for landslide susceptibility assessment in the Caspian forest, northern Iran. Int J Environ Sci Technol 11:909–926

Jibson RW, Keefer DK (1993) Analysis of the seismic origin of landslides: examples from the New Madrid seismic zone. Geol Soc Am Bull 105:521–536

Jibson RW, Harp EL, Schulz W, Keefer DK (2004) Landslides triggered by the 2002 M 7.9 Denali Fault, Alaska, earthquake and the inferred nature of the strong shaking. Earthq Spectra 20:669–691

Jibson RW, Harp EL, Schulz W, Keefer DK (2006) Large rock avalanches triggered by the M 7.9 Denali Fault, Alaska, earthquake of 3 November 2002. Eng Geol 83:144–160

Kaiser A, Holden C, Beavan J, Beetham D, Benites R, Celentano A, Collett D, Cousins J, Cubrinovski M, Dellow D, Denys P, Motagh M, Pondard N, McVerry G, Ristau J, Stirling M, Thomas J, Uma SR, Zhao J (2012) The M_w 6.2 Christchurch earthquake of February 2011: preliminary report. N Z J Geol Geophys 55:67–90

Kayen RE, Thompson E, Minasian D, Moss RES, Collins BD, Sitar N, Dreger D, Carver GA (2004) Geotechnical reconnaissance of the November 3, 2002 M 7.9 Denali Fault earthquake. Earthq Spectra 20:639–667

Keefer DK (1984) Landslides caused by earthquakes. Geol Soc Am Bull 95:406–421

Keefer DK (1993) The susceptibility of rock slopes to earthquake-induced failure. Assoc Eng Geol Bull 30:353–361

Keefer DK (1994) The importance of earthquake-induced landslides to long-term slope erosion and slope-failure hazards in seismically active regions. Geomorphology 10:265–284

Keefer DK (2000) Statistical analysis of an earthquake-induced landslide distribution—the 1989 Loma Prieta, California event. Eng Geol 58:231–249

Keefer DK (2002) Investigating landslides caused by earthquakes—a historical review. Surv Geophys 23:473–510

Khazai B, Sitar N (2004) Evaluation of factors controlling earthquake-induced landslides caused by Chi–Chi earthquake and comparison with the Northridge and Loma Prieta events. Eng Geol 71:79–95

Kieffer DS, Jibson R, Rathje EM, Kelson K (2006) Landslides triggered by the 2004 Niigata Ken Chuetsu, Japan, earthquake. Earthq Spectra 22:47–73

Korup O, Clague JJ, Hermanns RL, Hewitt K, Strom AL, Weidinger JT (2007) Giant landslides, topography, and erosion. Earth Planet Sci Lett 261:578–589

Lacombe O, Mouthereau F, Deffontaines B, Angelier J, Ch HT, Lee CT (1999) Geometry and quaternary kinematics of fold-and-thrust units of southwestern Taiwan. Tectonics 18:1198–1223

Li Y, Allen PA, Densmore AL, Xu Q (2003) Evolution of the Longmen Shan Foreland Basin (western Sichuan, China) during the Late Triassic Indosinian Orogeny. Basin Res 15:117–138

Li H, Wang H, Xu Z, Si J, Pei J, Li T, Huang Y, Song SR, Kuo LW, Sun Z, Chevalier ML, Liu D (2013a) Characteristics of the fault-related rocks, fault zones and the principal slip zone in the Wenchuan earthquake Fault Scientific Drilling Project Hole-1 (WFSD-1). Tectonophysics 584:23–42

Li W, Huang R, Tang C, Xu Q, Van Westen C (2013b) Co-seismic landslide inventory and susceptibility mapping in the 2008 Wenchuan earthquake disaster area, China. J Mt Sci 10:339–354

Lin A, Ren Z, Wu X (2009) Co-seismic thrusting rupture and slip distribution produced by the 2008 Mw 7.9 Wenchuan earthquake, China. Tectonophysics 471:203–215

Liu-Zeng J, Zhang Z, Wen L, Tapponnier P, Sun J, Xing X, Hu G, Xu Q, Zeng L, Ding L, Ji C, Hudnut KW, van der Woerd J (2009) Co-seismic ruptures of the 12 May 2008, Ms 8.0 Wenchuan earthquake, Sichuan: east–west crustal shortening on oblique, parallel thrusts along the eastern edge of Tibet. Earth Planet Sci Lett 286:355–370

Lu D, Cui J, Li X, Lian W (2010) Ground motion attenuation of Ms 8.0 Wenchuan earthquake. Earthq Sci 23:95–100

Mahdavifar MR, Solaymani S, Jafari MK (2006) Landslides triggered by the Avaj, Iran earthquake of June 22, 2002. Eng Geol 86:166–182

Malamud BD, Turcotte DL, Guzzetti F, Reichenbach P (2004) Landslides, earthquakes, and erosion. Earth Planet Sci Lett 229:45–59

Miles SB, Ho CL (1999) Rigorous landslide hazard zonation using Newmark's method and stochastic ground motion simulation. Soil Dyn Earthq Eng 18:305–323

Miles SB, Keefer DK (2007) Comprehensive area model of earthquake-induced landslides: technical specification and user guide. U.S. Geol Surv Open File Rep 2007-1072

Miles SB, Keefer DK (2009) Evaluation of CAMEL—comprehensive area model of earthquake-induced landslides. Eng Geol 104:1–15

Nakamura T, Tsuboi S, Kaneda Y, Yamanaka Y (2010) Rupture process of the 2008 Wenchuan, China earthquake inferred from teleseismic waveform inversion and forward modeling of broadband seismic waves. Tectonophysics 491:72–84

Newmark NM (1965) Effects of earthquakes on dams and embankments. Geotechnique 15:139–160

Nielsen SB (1998) Free surface effects on the propagation of dynamic rupture. Geophys Res Lett 25:125–128

Nishimura N, Yagi Y (2008) Rupture process for May 12, 2008 Sichuan Earthquake (Ver. 2) http://www.geol.tsukuba.ac.jp/~nisimura/20080512. Accessed 9 Jun 2011

Oglesby DD, Day SM (2002) Stochastic fault stress: implications for fault dynamics and ground motion. Bull Seismol Soc Am 92:3006–3021

Oglesby DD, Archuleta RJ, Nielsen SB (1998) Earthquakes on dipping faults: the effects of broken symmetry. Science 280:1055–1059

Oglesby DD, Archuleta RJ, Nielsen SB (2000a) Dynamics of dip-slip faulting: explorations in two dimensions. J Geophys Res 105:13643–13653

Oglesby DD, Archuleta RJ, Nielsen SB (2000b) The three dimensional dynamics of dipping faults. Bull Seismol Soc Am 90:616–628

Ouimet WB (2009) Landslides associated with the May 12, 2008 Wenchuan earthquake: implications for the erosion and tectonic evolution of the Longmen Shan. Tectonophysics 491:244–252

Owen LA, Kamp U, Khattak GA, Harp EL, Keefer DV, Bauer MA (2008) Landslides triggered by the 8 October 2005 Kashmir earthquake. Geomorphology 94:1–9

Parsons T, Chen J, Kirby E (2008) Stress changes from the 2008 Wenchuan earthquake and increased hazard in the Sichuan basin. Nature 454:509–510

Petit JP (1987) Criteria for the sense of movement on fault surfaces in brittle rocks. J Struc Geol 9:597–608

Plackett RL (1983) Karl Pearson and the Chi squared test. Int Stat Rev 51:59–72

Pourghasemi HR, Moradi HR, Fatemi Aghda SM, Gokceoglu C, Pradhan B (2014) GIS-based landslide susceptibility mapping with probabilistic likelihood ratio and spatial multi-criteria evaluation models (North of Tehran, Iran). Arab J Geosci 7:1857–1878

Regmi AD, Devkota KC, Yoshida K, Pradhan B, Pourghasemi HR, Kumamoto T, Akgun A (2014) Application of frequency ratio, statistical index, and weights-of-evidence models and their comparison in landslide susceptibility mapping in Central Nepal Himalaya. Arab J Geosci 7:725–742

Richardson N, Densmore AL, Seward D, Fowler A, Wipf M, Ellis MA, Li Y, Zhang Y (2008) Extraordinary denudation in the

Sichuan Basin: insights from low temperature thermochronology adjacent to the eastern margin of the Tibetan Plateau. J Geophys Res 113(B04409):1–23

Sato HP, Sekiguchi T, Kojiroi R, Suzuki Y, Iida M (2005) Overlaying landslides distribution on the earthquake source, geological and topographical data: the Mid Niigata prefecture earthquake in 2004, Japan. Landslides 2:143–152

Scheidegger AE (2001) Surface joint system. Tectonic stresses and geomorphology: a reconciliation of conflicting observations. Geomorphology 38:213–219

Shafer G (1976) A mathematical theory of evidence. Princeton University Press, Princeton

Shen ZK, Sun J, Zhang P, Wan Y, Wang M, Bürgmann R, Zeng Y, Gan W, Liao H, Wang Q (2009) Slip maxima at fault junctions and rupturing of barriers during the 2008 Wenchuan earthquake. Nat Geosci 2:718–724

Shi Z, Day SM (2013) Rupture dynamics and ground motion from 3-D rough-fault simulations. J Geophys Res Sol Ea 118:1122–1141

Shi B, Anooshehpoor A, Brune JN, Zeng Y (1998) Dynamics of thrust faulting: 2D lattice model. Bull Seismol Soc Am 88:1484–1494

Shou KJ, Wang CF (2003) Analysis of the Chiufengershan landslide triggered by the 1999 Chi–Chi earthquake in Taiwan. Eng Geol 68:237–250

Somerville P, Irikura K, Graves R, Sawada S, Wald D, Abrahamson N, Iwasaki Y, Kagawa T, Smith N, Kowada A (1999) Characterizing crustal earthquake slip models for the prediction of strong ground motion. Seismol Res Lett 70:59–80

Song Y, Gong J, Gao S, Wang D, Cui T, Li Y, Wei B (2012) Susceptibility assessment of earthquake-induced landslides using Bayesian network: a case study in Beichuan, China. Comput Geosci 42:189–199

Tang H, Jia H, Hu J, Li D, Xiong C (2010) Characteristics of landslides induced by the great Wenchuan earthquake. J Earth Sci 21:104–113

Tesón E, Mora A, Silva A, Namson J, Teixell A, Castellanos J, Casallas W, Julivert M, Taylor M, Ibáñez-Mejía, Valencia VA (2013) Relationship of Mesozoic graben development, stress, shortening magnitude, and structural style in the Eastern Cordillera of the Colombian Andes. Geol Soc Lond Spec Pub 377:257–283

Ulusay R, Tuncay E, Sonmez H, Gokceoglu C (2004) An attenuation relationship based on Turkish strong motion data and iso-acceleration map of Turkey. Eng Geol 74:265–291

USGS (2008) Magnitude 7.9—Eastern Sichuan, China, 2008 May 12 06:28:01 UTC. United States Geological Survey (USGS), http://earthquake.usgs.gov/earthquakes/eqinthenews/2008/us2008ryan/

Vearncombe J, Vearncombe S (1999) The spatial distribution of mineralization: applications of Fry analysis. Econ Geol 94:475–486

Velasco AA, Ammon CJ, Farrell J, Pankow K (2004) Rupture directivity of the 3 November 2002 Denali fault earthquake determined from surface waves. Bull Seismol Soc Am 94(6B):293–299

Wan Y, Shen ZK (2010) Static Coulomb stress changes on faults caused by the 2008 Mw 7.9 Wenchuan, China earthquake. Tectonophysics 491:105–118

Wang KL, Lin ML (2010) Development of shallow seismic landslide potential map based on Newmark's displacement: the case study of Chi–Chi earthquake, Taiwan. Environ Earth Sci 60:775–785

Wang H, Wang G, Wang F, Sassa K, Chen Y (2008a) Probabilistic modeling of seismically triggered landslides using Monte Carlo simulations. Landslides 5:387–395

Wang Y, Wang E, Shen Z, Wang M, Gan W, Qiao X, Meng G, Li T, Tao W, Yang Y, Cheng J, Li P (2008b) GPS-constrained inversion of present-day slip rates along major faults of the Sichuan-Yunnan region, China. Sci China Earth Sci 51:1267–1283

Wang Z, Fukao Y, Pei S (2009) Structural control of rupturing of the Mw 7.9 2008 Wenchuan earthquake, China. Earth Planet Sci Lett 279:131–138

Wang X, Nie G, Wang D (2010) Relationships between ground motion parameters and landslides induced by Wenchuan earthquake. Earthq Sci 23:233–242

Wang H, Li H, Si J, Sun Z, Huang Y (2014) Internal structure of the Wenchuan earthquake fault zone, revealed by surface outcrop and WFSD-1 drilling core investigation. Tectonophysics 619–620:101–114

Wei S, Graves R, Helmberger D, Avouac JP, Jang J (2012) Sources of shaking and flooding during the Tohoku-Oki earthquake: a mixture of rupture styles. Earth Planet Sci Lett 333–334:91–100

Wells DI, Coppersmith KJ (1994) New empirical relationships among magnitude, rupture length, rupture width, rupture area, and surface displacement. Bull Seismol Soc Am 84:974–1002

Wilson RC, Keefer DK (1985) Predicting areal limits of earthquake-induced landsliding. In: Ziony JI (eds) Evaluating earthquake hazards in the Los Angeles Region—an earth-science perspective. U.S. Geol Surv Prof Paper 1360:316–345

Wu JH, Chen CH (2011) Application of DDA to simulate characteristics of the Tsaoling landslide. Comput Geotech 38:741–750

Wu JH, Lin HM (2009) Analyzing the shear strength parameters of the Chiu-fen-erh-shan landslide: integrating strong-motion and GPS data to determine the best-fit accelerogram. GPS Solut 13:153–163

Wu JH, Tsai PH (2011) New dynamic procedure for back-calculating the shear strength parameters of large landslides. Eng Geol 123:129–147

Wu JH, Lin JS, Chen CS (2009) Dynamic discrete analysis of an earthquake-induced large-scale landslide. Int J Rock Mech Min Serv 46:397–407

Xu C, Xu X (2013) Controlling parameter analyses and hazard mapping for earthquake-triggered landslides: an example from a square region in Beichuan County, Sichuan Province, China. Arab J Geosci 6:3827–3839

Xu C, Xu X (2014) Statistical analysis of landslides caused by the Mw 6.9 Yushu, China, earthquake of April 14, 2010. Nat Hazards 72:871–893

Xu X, Wen X, Yu G, Chen G, Klinger Y, Hubbard J, Shaw J (2009) Coseismic reverse- and oblique-slip surface faulting generated by the 2008 Mw 7.9 Wenchuan earthquake, China. Geology 37:515–518

Xu C, Xu W, Dai F, Sard AK (2012) Comparison of different models for susceptibility mapping of earthquake triggered landslides related with the 2008 Wenchuan earthquake in China. Comput Geosci 46:317–329

Xu C, Xu X, Yao X, Dai F (2014) Three (nearly) complete inventories of landslides triggered by the May 12, 2008 Wenchuan Mw 7.9 earthquake of China and their spatial distribution statistical analysis. Landslides 11:441–461

Yang JS (1992) Landslide mapping and major earthquakes on the Kakapo Fault, South Island, New Zealand. J R Soc N Z 22:205–212

Yin Y (2014) Vertical acceleration effect on landsides triggered by the Wenchuan earthquake, China. Environ Earth Sci 71:4703–4714

Yin J, Chen J, Wang X, Zheng Y (2010) The characteristics of the landslides triggered by the Wenchuan Ms 8.0 earthquake from Anxian to Beichuan. J Asian Earth Sci 37:452–459

Yu YX, Gao MT (2001) Effects of the hanging wall and footwall on peak acceleration during the Jiji (Chi–Chi), Taiwan Province, earthquake. Acta Seismol Sin 14:654–659

Zhang W, Shen Y, Chen XF (2008) Numerical simulation of strong ground motion for the Ms 8.0 Wenchuan earthquake of 12 May 2008. Sci China Earth Sci 51:1637–1682

Zhang PZ, Wen X, Shen ZK, Chen J (2010) Oblique, high-angle, listric-reverse faulting and associated development of strain: the Wenchuan earthquake of May 12, 2008, Sichuan, China. Annu Rev Earth Planet Sci 38:353–382

Zhao CP, Chen ZL, Zhou LQ, Li ZX, Kang Y (2010) Rupture process of the Wenchuan M 8.0 earthquake of Sichuan, China: the segmentation feature. Chin Sci Bull 55:284–292

Zhao W, Huang R, Ju N, Zhao J (2014) Assessment model for earthquake-triggered landslides based on quantification theory I: case study of Jushui River basin in Sichuan, China. Nat Hazards 70:821–838

Zhou D, Graham SA (1996) Songpan-Ganzi Triassic flysch complex of the West Qinling Shan as a remnant ocean basin. In: Yin A, Harrison M (eds) The tectonic evolution of Asia. Cambridge University Press, Cambridge, pp 281–299

Zhuang J, Cui P, Hu K, Chen X, Ge Y (2010) Characteristics of earthquake-triggered landslides and post-earthquake debris flows in Beichuan County. J Mt Sci 7:246–254